SEDIMENTOLOGY the journal of the International Association of Sedimentologists IAS

Sedimentology (2024) **71**, 1709–1743 doi: 10.1111/sed.13219

Flow-induced interfacial deformation structures (FIDS): Implications for the interpretation of palaeocurrents, flow dynamics and substrate rheology

JEFF PEAKALL*, JAMES L. BEST†,‡,§,¶, JACO H. BAAS**, PAUL B. WIGNALL*, DAVID M. HODGSON* and PIOTR ŁAPCIK††

**School of Earth and Environment, University of Leeds, Leeds LS2 9JT, UK (E-mail: j.peakall@leeds.ac.uk)*

†Department of Earth Science and Environmental Change, University of Illinois at Urbana-Champaign, Urbana, IL 61801, USA

‡Department of Geography and GIS, University of Illinois at Urbana-Champaign, Urbana, IL 61801, USA

§Department of Mechanical Science and Engineering, University of Illinois at Urbana-Champaign, Urbana, IL 61801, USA

¶Ven Te Chow Hydrosystems Laboratory, University of Illinois at Urbana-Champaign, Urbana, IL 61801, USA

***School of Ocean Sciences, Bangor University, Menai Bridge LL59 5AB, UK*

††Institute of Geological Sciences, Jagiellonian University, Gronostajowa 3a, Kraków PL-30-387, Poland

Associate Editor – Fabrizio Felletti

ABSTRACT

Sole structures on the base of turbidites, and other bed types, are typically classified into scour marks and tool marks, such as flutes, grooves, skim marks and prod marks. Yet, there are a range of other common sole marks that are unrelated to scouring or tools, and whose origin is poorly understood. Prominent among these sole structures are longitudinal ridges and furrows, and 'dinosaur leather' structures associated with mud ripples. Herein, these features are described and it is argued that they are the product of deformation of the substrate during a sediment gravity flow event. In these flow-induced interfacial deformation structures (FIDS), a soft cohesive substrate undergoes deformation in response to a buoyant force induced by the denser basal component of an overriding flow, and the flow interacts with this buoyant deformation through shear to remould the substrate. Variations in the relative strength of these buoyant and shear-induced forces explain the wide range of FIDS that can form. This FIDS model reinterprets the formation of longitudinal ridges and furrows, which have previously been classified as scour marks, and explains their distinctive spatial patterns. Furthermore, the new model builds on the seminal work of Dżułyński and colleagues in the 1960s and 1970s, who identified that these structures contain key palaeocurrent information, and it is argued that such information is largely under-utilized. Importantly, alongside their utility as palaeocurrent indicators, FIDS provide insights into the rheology of the substrate at the time of their formation, and thus the nature of basal flow conditions in the formative flows.

Keywords Longitudinal ridges and furrows, mud ripple, sediment gravity flows, sole mark, transitional flow.

INTRODUCTION

Sole structures in deep-marine environments are a class of sedimentary structure that have received remarkably limited research since the early 1970s, and whose utility has been largely restricted to the collection of palaeocurrent information (Peakall *et al.*, 2020). However, recent work has demonstrated that flutes and tool marks can provide information concerning the nature of the formative flows and the rheology of the substrate (Peakall *et al.*, 2020; Baas *et al.*, 2021a; McGowan *et al.*, 2024). Yet, there remain a range of sole structures that have not been re-examined since the pioneering work of Dżułyński and co-workers (e.g. Dżułyński & Walton, 1963, 1965; Dżułyński, 1965, 1966; Dżułyński & Simpson, 1966a, 1966b) and Allen (1969, 1971a) in the 1960s and early 1970s. Chief among these are *longitudinal ridges and furrows*, and the *scales* — updip closing arcs — that can occur within, or occur separate to, these ridges and furrows (Fig. 1A and B; Craig & Walton, 1962; Dżułyński & Walton, 1965). There are also a range of orientated and non-orientated structures, including *polygonal forms*, and this combination of structures can ornament mud ripples, sometimes producing spectacular surfaces termed 'dinosaur leather' (Fig. 1D; Chadwick, 1948). Lastly, *transverse wrinkles* (*sensu* Dżułyński & Sanders, 1962) are considered (Fig. 1C). The present paper revisits each of these structures in turn, and proposes a process-based model that clarifies the origin and relationship between these different structures. The new model has implications for the utility of these sedimentary structures in terms of palaeocurrents, flow dynamics and as measures of substrate strength.

SEDIMENTARY STRUCTURES: CHARACTERISTICS AND FORMATIVE PROCESSES

Longitudinal ridges and furrows

Characteristics

Longitudinal ridges and furrows (also called ridge-and-furrow moulds; Allen, 1982) occur as a series of regularly spaced (millimetres to tens of millimetres wide) ridges and furrows with an overall parallel-to-flow fabric that provides a unidirectional or bidirectional palaeocurrent indicator (Dżułyński & Walton, 1965; Collinson & Mountney, 2019; Figs 1A and 2). This parallel-to-flow nature is confirmed by rare contemporaneous sole marks such as grooves, flutes (Dżułyński & Walton, 1965) and prod marks (Fig. 2C). In cross-section, furrows are shallow and flat-bottomed, or deeper and rounded, and sand-filled (commonly millimetres to tens of millimetres in depth), with sharper ridges between them (formed of mud originally, though typically seen as erosional relief on the base of sandstones), reflecting troughs and sharp ridges on the original mud bed (Dżułyński & Walton, 1965; Allen, 1982). Individual furrows typically initiate as rounded, convex-upstream forms and terminate longitudinally, either tapering, or via more rounded concave-upstream forms (Fig. 1A). A unidirectional flow direction is indicated where these convex-upstream forms can be recognized (Collinson & Mountney, 2019). Furrows are typically hundreds of millimetres long, and do not exhibit a constant width (Figs 1A and 2), in some cases forming a series of bulbous protrusions, as seen in planform, along their length (Figs 1A and 2A); likewise, ridges do not maintain a constant width (Figs 1A and 2A). Ridges and furrows are frequently slightly sinuous, and occasionally highly sinuous, in planform, and in places can exhibit dendritic patterns (Figs 1A and 2C). In some examples, in cross-sectional view, the mud ridges exhibit flames (Kelling & Walton, 1957). Longitudinal ridges and furrows tend to cover the entire base of the bed, and in exceptional exposures can show larger-scale patterns of convergence and divergence (Allen, 1982, fig. 1.25). Ridges and furrows can: (i) form independently; (ii) form at the same time as flutes and tool marks; or (iii) be cut later by flutes and tool marks (Dżułyński & Walton, 1965). Longitudinal ridges and furrows are typically found on the soles of thin (a few tens of millimetres), fine-grained, turbiditic sands (Allen, 1971b, 1982). In many cases, longitudinal furrows also exhibit arrays of cuspate features (scales), composed of sand, separated by thin mud layers, within the individual furrows that widen downstream, thus providing a palaeocurrent direction (Craig & Walton, 1962). The origin of these 'scales' (*sensu* Craig & Walton, 1962) is examined after consideration of the formative processes of longitudinal ridges and furrows below.

Formative mechanisms

A number of formative mechanisms of longitudinal ridges and furrows have been postulated in the literature.

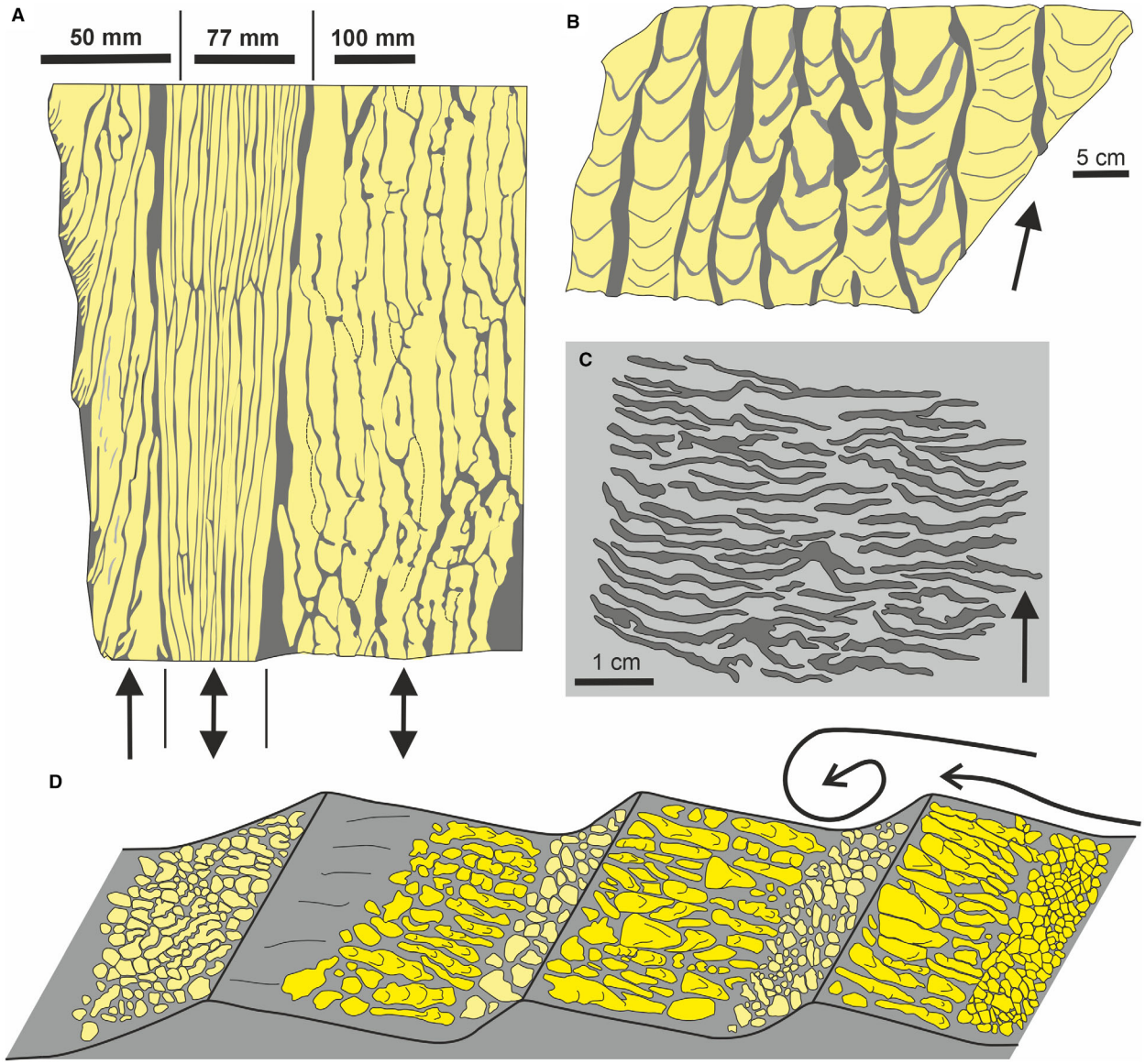

Fig. 1. Schematic morphologies of flow-induced interfacial deformation structures (FIDS). (A) Longitudinal ridges and furrows; sand shown in yellow and mud in grey. Three different morphologies are shown from left to right; partially dendritic (see Fig. 2C), elongated and slightly sinuous (see Fig. 2B) and wider and shorter forms (see Fig. 2A). Black arrows show unidirectional (dendritic) and bidirectional flow indicators. (B) Scales; sand is shown in yellow, mud in ridges between furrows in dark grey, and mud between scales in lighter grey. A range of different scale morphologies are shown within the figure, including symmetrical and asymmetrical forms, and variations in the amount of mud between scales (see Fig. 7 for photos). (C) Transverse wrinkles, shown in dark grey, and surrounding mud in lighter grey (see Fig. 10). (D) FIDS on mud ripples. Morphologies are shown with reference to the three-dimensional geometry of mud ripples during formation; however they are found on the base of sandstones and thus are inverted relative to the figure. Flow direction shown by arrows, including the recirculation zone in the lee of the ripples; the latter is shown schematically, with the dimensions of the recirculation zone altering as a function of flow cohesitivity (see Baas & Best, 2008). A range of FIDS morphologies is illustrated: far right – polygonal forms in the trough, with more longitudinal forms on the stoss side, some displaying scales; centre – similar but with equant, but less polygonal, forms on the lee and in the trough; left – showing the upper stoss as smooth. Darker yellow on stoss side and lighter yellow on lee side of mud ripples, respectively. Mud-ripple wavelengths range from 0.02 to 0.40 m.

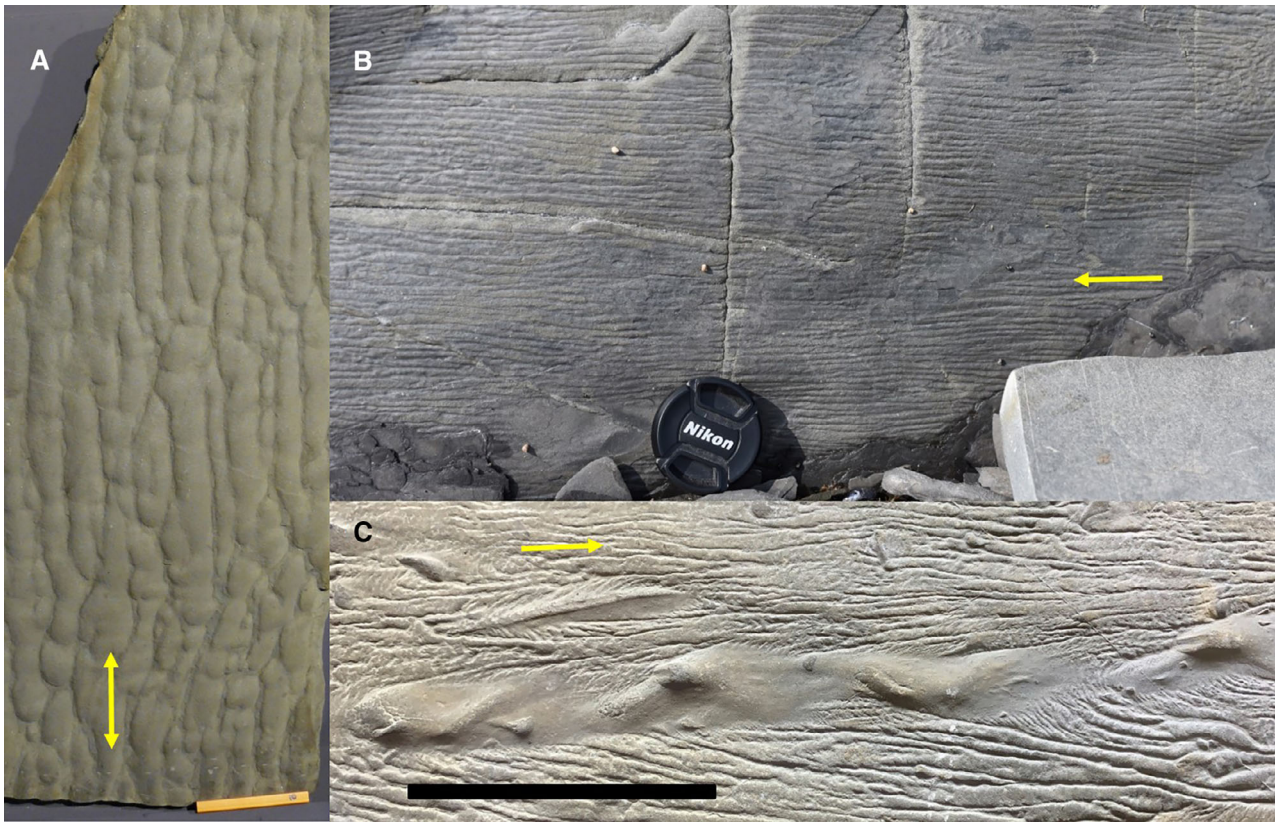

Fig. 2. Examples of longitudinal ridges and furrows. (A) Example showing furrows that are relatively short in a longitudinal direction, with bulbous projections along their length, and marked changes in furrow width. Oligocene, Krosno beds, Poland. Yellow scale bar is 100 mm long. Yellow arrow shows bidirectional flow direction. (B) Slightly sinuous and elongate ridges and furrows; middle Ordovician Cloridorme Formation, Gaspé Peninsula, Quebec, Canada. Lens cap for scale, diameter 77 mm. Yellow arrow shows flow direction, however, this is obtained from other information, and the longitudinal ridges and furrows only give a bidirectional indicator. (C) Longitudinal ridges and furrows exhibiting dendritic patterns, best seen where they terminate against the edges of prod marks, with the latter showing flute marks at their downstream ends; flow from left to right. In places, the prod marks cut the ridges and furrows, whilst elsewhere the ridges and furrows deform around the prod marks, showing that the two structures thus formed contemporaneously. Oligocene, Krosno beds, Poland. Black scale bar is 100 mm long. Yellow arrow gives flow direction. Examples (A) and (C) are from samples in the collection of the Natural Sciences Education Centre at the Jagiellonian University, Kraków, Poland.

Formative mechanism 1: Helicoidal scour

The prevailing interpretation for longitudinal ridges and furrows is that they are pure scour structures (e.g. Reineck & Singh, 1980; Allen, 1982; Stow, 2005; Bridge & Demicco, 2008; Nichols, 2009; Leeder, 2011; Collinson & Mountney, 2019), with a scour origin first proposed by Craig & Walton (1962). Dżułyński & Walton (1963) suggested that they were formed by helicoidal flows close to the bed, and Dżułyński (1965, 1966) later suggested that these flows were the product of twin, counter-rotating, helicoidal flow cells. The experiments of Allen (1971a), using flows that slowly dissolved plaster-of-Paris (over *ca* four to eleven days), supported this model of paired counter-rotating vortices. Where fluid circulating in the cells was directed downward, amplified velocity fluctuations were present, and thus greater dissolution occurred (Allen, 1966), whilst upward flow led to lower velocity fluctuations, reduced dissolution and the development of ridges (Allen, 1971a). For clay beds, enhanced basal shear stress will produce greater erosion under the descending parts of cells, and reduced shear stress and erosion under upward flow (Allen, 1971a). Once formed, topographically-forced helicoidal flow over these initial ridges and furrows may promote their further development. The ridges and furrows in the plaster-of-Paris experiments of Allen (1966, 1971a) were

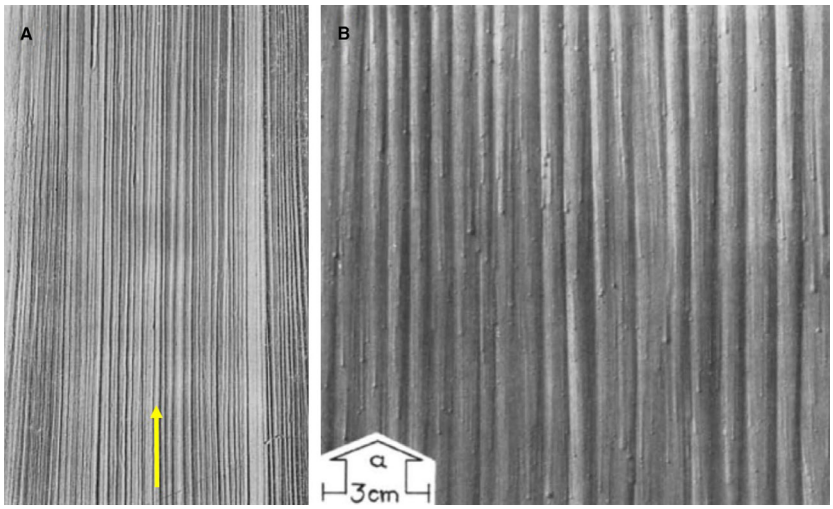

Fig. 3. (A) Rectilinear grooves formed in clay beds; width of bed shown is 0.27 m (used with permission of SEPM, from Allen, 1969, *J. Sed. Petr.*, 39, 607–623; permission conveyed through Copyright Clearance Center Inc.). Yellow arrow gives flow direction. (B) 'Longitudinal ridges and furrows' formed in plaster-of-Paris (from Allen, 1971a, reproduced with permission of Elsevier). Arrow at bottom left gives flow direction.

strongly rectilinear with little variation in width or depth (Fig. 3B; Allen, 1971a, fig. 75). In some runs, however, longitudinal changes in the width and depth of the troughs and ridges were present, together with the development of a planform sinuosity (Allen, 1971a, fig. 77), which was assumed to be the product of secondary transverse instabilities in the flow.

Allen (1969) also undertook experiments using beds made of kaolin clay settled over a few days, and described as 'weakly cohesive'. Water contents were 53 to 59% by weight, equivalent to bed densities (strengths) that correspond to hard mud in the classification scheme of van Rijn (1993). This bed density is typically representative of ≥100 years of mud consolidation, at odds with the several days of settling and consolidation. Note that allowance was made for the fact that kaolinite is a weaker clay than the mixed clays of van Rijn's (1993) classification (see McGowan *et al.*, 2024). Furthermore, Allen (1969) noted that the upper few millimetres were very weakly cohesive, and the very top of the bed was almost 'soup-like'. These experiments produced 'rectilinear longitudinal grooves', <1.5 mm deep and spaced 2 to 30 mm apart, at low velocities (*ca* 0.20 to 0.30 m s^{-1}), which formed via low erosion rates over *ca* 2 to 6 h (Fig. 3A). Allen (1969) stated that these almost perfectly straight, closely spaced, lineations had no known analogues in the geological record. However, Allen (1971a) later suggested that they might correspond to the longitudinal ridges and furrows observed in the plaster-of-Paris experiments. At higher velocities (*ca* 0.35 to 0.45 m s^{-1}), 'meandering grooves' were formed in the kaolin beds, which Allen (1971a) suggested may be analogous to more sinuous longitudinal ridges and furrows seen in the same plaster-of-Paris experiments. These meandering grooves, however, are far more analogous to sinuous rill moulds, albeit these are rare in the rock record (e.g. Dżułyński & Sanders, 1962).

Allen (1969, 1971a) argued that the initiation and spacing of the ridges and furrows was a product of streaks in the laminar sublayer of turbulent flows (e.g. Kline *et al.*, 1967). Streaks are the slow-velocity zones in the lower boundary layer coupled to hairpin vortices, and may be expected to align with the ridges. Periodic sweeps, that are the flow-parallel, high-velocity, corridors of fluid in the lower boundary layer, occur between these low-speed streaks, and in this model would help to account for the preferential erosion of the bed in the furrows (e.g. Best, 1992). The spacing of these streaks is a function of the shear velocity and fluid viscosity, which at the entrainment threshold of motion for muds to sands yields lateral spacings of *ca* <10 mm (Best, 1992), although the presence of clays in the flow will alter streak spacing in drag reducing (Best & Leeder, 1993) and transitional (Baas *et al.*, 2009, 2016a) flows. Allen (1971a) hypothesized that these streaks are then locked into position by the

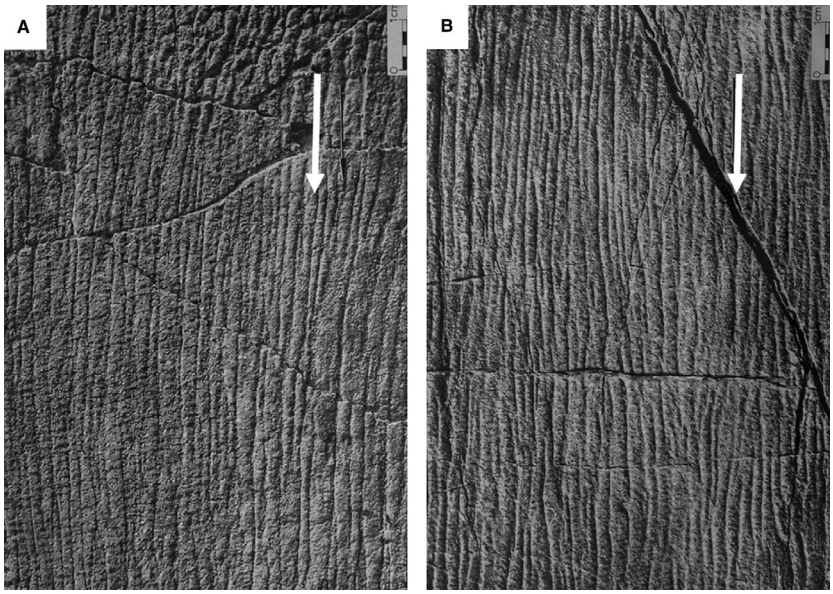

Fig. 4. (A) Experimental longitudinal ridges and furrows, and (B) Longitudinal ridges and furrows as seen in outcrop; from Dżułyński & Walton (1965) reproduced with permission of Elsevier. White arrows show flow direction.

development of the ridges and furrows, as also speculated for the impact of flow-orientated ridges in mobile sands (Best, 1992).

In summary, experiments that propose scour as the formative mechanism for longitudinal ridges and furrows have been based either on long-term dissolution processes (plaster-of-Paris) that are not directly applicable to muddy substrates, or generated features that formed slowly (over hours) in weakly cohesive mud. In addition, the resultant structures in these clay beds are strongly rectilinear, and are in marked contrast to field observations that show furrows terminate longitudinally over short distances, and do not maintain a constant width and depth. The lateral spacing of furrows may also be greater than streak-induced furrows formed in the lower boundary layer.

Formative mechanism 2: Density differences and helicoidal flow

Experiments using suspensions of plaster-of-Paris, run over soft mud beds, have produced remarkably similar forms to those seen in longitudinal ridges and furrows in the rock record (Fig. 4; Dżułyński, 1965; Dżułyński & Walton, 1965). The details for these experiments are limited, with no flow or substrate measurements (e.g. Dżułyński & Walton, 1963, 1965); indeed, in some cases, no experimental details are provided (e.g. Dżułyński, 1965; Anketell *et al.*, 1970). However, based on details provided in earlier papers, some aspects of the flow rheology can be estimated (Peakall *et al.*, 2020). The plaster-of-Paris flows, where reported, had densities of *ca* 1260 to 1520 kg m^{-3}, viscosities around 1.0 to 2.5 Pa s^{-1}, and likely exhibited a yield strength. These are thus analogous to transitional plug flows (*sensu* Baas *et al.*, 2009), or intermediate strength debris flows (*sensu* Talling, 2013), rather than turbidity currents as envisaged by the original workers (see discussion in Peakall *et al.*, 2020). The plaster-of-Paris flows were run over a mud bed that had typically formed from kaolin suspensions settled over several days (Dżułyński & Walton, 1965). A qualitative estimate of bed density can be provided by comparison to consolidation periods of natural clays in the classification scheme of van Rijn (1993), with experiments likely representative of the 'weakly consolidated fluid mud' category, equivalent to *ca* one week of consolidation, and bed densities of 1050 to 1150 kg m^{-3}.

Anketell *et al.* (1970) generated longitudinal ridges and furrows in experiments with reversed density differences, where the upper layer, in this case the flow, had a higher density than the underlying substrate (as was the case for the earlier experiments of Dżułyński and co-workers). Anketell *et al.* (1970) argued that longitudinal ridges and furrows are produced as a result of vertical deformation of the substrate, in combination with the influence of a horizontal flow, and stated that where the: "horizontal

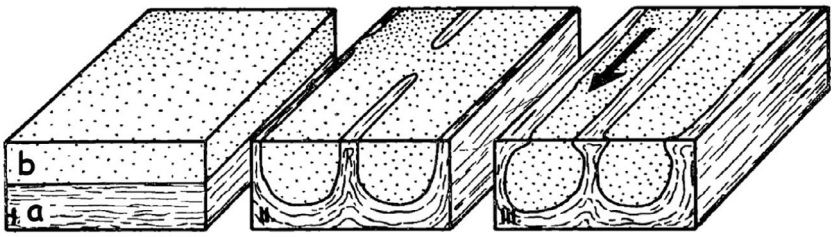

Fig. 5. Model for the formation of longitudinal ridges and furrows. Layer 'a' is the substrate and has a lower density, and higher viscosity, than the overlying flowing layer 'b', resulting in the diapir-like development of elongate ridges of layer 'a'. Black arrow shows flow direction. Adapted from Anketell *et al.* (1970) and reproduced with permission of Annales Societatis Geologorum Poloniae.

component [of deformation] predominates the interface is directly deformed into a set of longitudinal ridges trending parallel to the direction of movement". The flow component was linked to the development of counter-rotating helicoidal flow cells (Dżułyński & Simpson, 1966a; Dżułyński, 1996). The evidence presented by Anketell *et al.* (1970) consists of a single sketch of the process (Fig. 5), alongside reference to the earlier experiments of Dżułyński and co-workers. Consequently, it is unclear to what degree the deformation process could be observed, or how much of the deformation in experiments such as those of Dżułyński (1965; Fig. 4) occurred during flow, and how much was post-depositional.

The model of Anketell *et al.* (1970) builds on earlier conceptual ideas of the development of longitudinal ridges, and scales (Dżułyński & Simpson, 1966a, 1966b), based on experiments examining instabilities in air flows with reversed density gradients and horizontal shear (Graham, 1933). The background to these temperature-driven convection experiments is described in more detail in the section below concerning *Scales*. However, the emphasis in these previous papers on sole marks remains on the: "longitudinal ridges [being] produced by shear drag acting normal to the main flow" (Dżułyński & Simpson, 1966a) and as a result of: "compression arising from current shear" (Dżułyński & Simpson, 1966b), rather than from buoyancy-driven diapirism. Furthermore, Dżułyński (1996) summarized that, for longitudinal ridges and furrows with closely spaced sets of ridges, the flows are: "indicative of relatively rapid flow and relatively low density of the settling suspension". This contention is used more widely (e.g. Dirnerová & Janočko, 2014), but is at odds with consideration of reversed density systems, and the physical experiments themselves. However, the experiments were always considered as turbidity currents by the original authors, rather than dense currents more typical of intermediate debris flows (transitional plug flows) that the flows actually represented, as revealed in recent research (Peakall *et al.*, 2020).

Formative mechanism 3: Mechanical deformation

Anketell *et al.* (1970) undertook an experiment with a poorly consolidated clay layer over a more consolidated layer, with the upper layer thus less dense and less viscous than the underlying layer. A cylinder was then rolled across the surface, producing sharp crested longitudinal ridges and furrows, (Fig. 6), termed dendritic ridges (Dżułyński & Walton, 1963). The mechanical compaction forces the lighter layer into the denser one, and the denser layer rises as a series of ridges. The denser material adheres to the roller and is thus pulled up above the surrounding layer (Anketell *et al.*, 1970). In natural systems, compaction by a dense overriding flow, such as a debris flow where the plug flow component directly intersects the bed (laminar plug flow, *sensu* Peakall *et al.*, 2020), is unlikely to exhibit this adherence of material. Furthermore, a laminar plug flow might be expected to erode the low-density layer. Assuming that no, or limited, erosion takes place, then it is possible to envisage a case where the still relatively poorly consolidated overlying layer is subsequently eroded to reveal the ridges, prior to the deposition of a sand layer.

Formative mechanism 4: Formation by lobes and clefts

Experiments with a slow-moving front of water over a weak clay bed produced ridges whose spacing was the same as the crenulations at the front of the flow (Dżułyński & Walton, 1963). Allen (1971b, 1982) later postulated that these

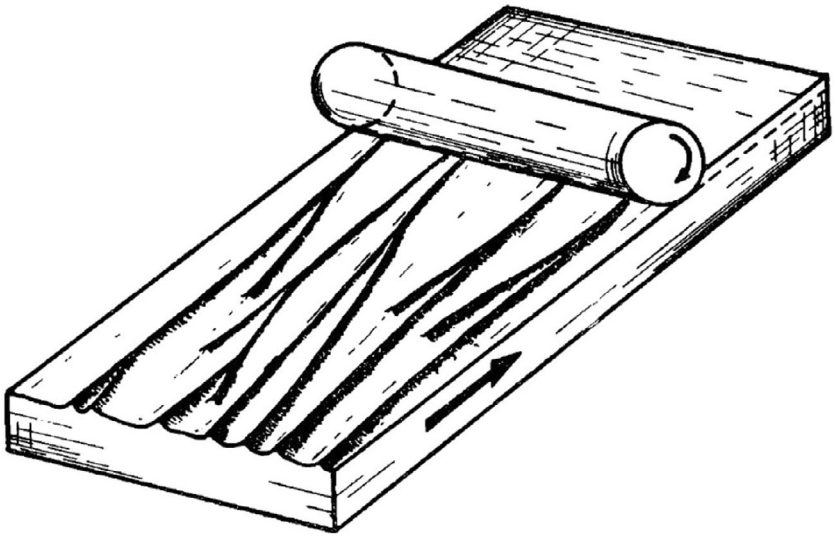

Fig. 6. Formation of sharp-crested longitudinal ridges and furrows via mechanical compaction generated by a rolled cylinder. Black arrow shows flow direction. From Anketell *et al.* (1970) reproduced with permission of Annales Societatis Geologorum Poloniae.

might be linked to lobes and clefts at the front of turbidity currents, and their expression within the flow behind the head of a density current. The observation that clefts occur at multiple scales was suggested as a mechanism for explaining more complex patterns of longitudinal ridges and furrows (Allen, 1982). However, experiments have shown that lobe width scales with the depth of the flow and the flow Reynolds number (Simpson, 1972), suggesting that flows would have to be small (equivalent to laboratory size currents) to have generated typical longitudinal ridges and swales, given their widths (Allen, 1971b). Lobe width is approximately one or two times the flow depth in geophysical-scale gravity currents, and apparently independent of Reynolds number (Dai & Huang, 2022), further suggesting that the formation of longitudinal ridges and furrows would need to be the product of very small flows. Observations of the planform development and merging of clefts (Simpson, 1972, fig. 8; Dai & Huang, 2022, fig. 4) also bear little comparison to the comparatively straight and elongate nature of longitudinal ridges and furrows.

Discussion of mechanisms

The experiments of Dżułyński (1965) and Dżułyński & Walton (1965) produced structures highly analogous to natural longitudinal ridges and furrows (Fig. 4). This is in contrast to the scour features in the experiments of Allen (1969) with clay beds, which were strongly rectilinear relative to typical longitudinal ridges and furrows. Similarly, the dissolution-based experiments produced ridges and furrows that are also strongly linear (Allen, 1971a). Where transverse instabilities developed, the resulting structures show evidence for merging of furrows and more variable width, and thus are more comparable to longitudinal ridges and furrows. However, these are unstable and ultimately generate local transverse instabilities that develop into flute casts (Allen, 1971a). Whilst the experiments of Dżułyński (1965) and Dżułyński & Walton (1965) are highly analogous in form, their formative mechanisms are less clear, with Dżułyński's (1996) overview describing, but not critically assessing, the four mechanisms detailed above. Consequently, the interpretation of longitudinal ridges and furrows has remained as scour structures, following their classification as such in 1962 (Craig & Walton, 1962; see also Dżułyński & Walton, 1965, table III).

The dimensions of the tanks, and the velocity of the flows, in the experiments of Dżułyński and co-workers were not given, although they were described as 'small tanks' (images of sole structures are <0.50 m in length; Dżułyński & Walton, 1965). Records from the Jagiellonian University show that one of the tanks had dimensions of 0.65 m long, 0.15 m wide and 0.16 m high; the second tank was larger but details are lacking. Given tanks of 0.65 m length, and possibly up to several metres, the sediment gravity flows likely took just tens of seconds, to perhaps a few minutes, to traverse them. Consequently, the longitudinal ridges and furrows were produced very rapidly, albeit that an unknown amount of additional deformation may have occurred post-deposition. This rapid development is at odds with the pure-scour

experiments of Allen (1969) that took several hours to develop. If scour were the key process in the experiments of Dżułyński and co-workers, then complex patterns were also formed very rapidly. In addition, no products of erosion were noted in the experiments, such as material being pushed ahead of the flow, nor are there observations of deposits when the plaster-of-Paris was removed, enabling the sole structures to be observed. Consequently, pure scour by helicoidal flows appears improbable in these experiments. Formation by lobes and clefts would also appear unlikely, given that the spatial distribution of clefts bears little similarity to longitudinal ridges and furrows, and this process would again rely upon erosional scour.

This leaves the two mechanisms associated with vertical deformation of the substrate, based on the work of Dżułyński & Simpson (1966a, 1966b) and Anketell *et al.* (1970). Given that the examples concerning sediment gravity flows are associated with reversed density gradients where the flow is denser than the substrate (Dżułyński, 1965; Dżułyński & Walton, 1965), this suggests that the features are formed by a combination of flow-induced and buoyancy-induced deformation, as postulated initially by Dżułyński & Simpson (1966a, 1966b) and later by Anketell *et al.* (1970), rather than purely by flow-induced mechanical deformation squeezing the bed. The presence of ridges with flames in some field examples (Kelling & Walton, 1957; Dżułyński & Walton, 1965) also suggests a muddy substrate undergoing buoyancy-induced diapirism, because it is difficult to envisage how such features can be formed through scouring. Lateral shear drag normal to the flow, and compression arising from the current shear have both been postulated for bed deformation (Dżułyński & Simpson, 1966a, 1966b). However, the induced shear from counter-rotating flow cells with a width of millimetres to tens of millimetres is likely to be very small. By contrast, the buoyancy forces in the experiments of Dżułyński & Simpson (1966a, 1966b) induced by the difference in density of a recently settled clay bed, estimated at 1050 to 1150 kg m^{-3} and the flow at 1260 to 1520 kg m^{-3}, are likely to have been appreciable.

Numerical modelling of reversed-density structures, exhibiting buoyancy in the absence of a flow, suggests that the wavelength (width) of the diapiric structures is a function of the density and viscosity difference between the two layers, with wavelength decreasing with increasing density difference and with increasing viscosity difference (Harrison & Maltman, 2003). Therefore, the characteristically small widths of the ridges and furrows (millimetres to tens of millimetres) suggests that the density difference between flow and substrate is typically high (viscosity will likewise likely scale with the density difference – see the *Scales* section), in keeping with the experiments of Dżułyński (1965) and Dżułyński & Walton (1965).

Scales

Characteristics

Scales (*sensu* Craig & Walton, 1962), or scaly structures, are often associated with longitudinal ridges and furrows, either as relatively isolated examples within furrows, or as arrays that cover the entire surface of the furrows (Fig. 1B). Individual scales are cuspate and resemble small flutes in planform, and like flutes indicate the flow direction, with flow being in the direction that the cusps widen (Craig & Walton, 1962). Scales in adjacent furrows, can either be offset to one another in the downstream direction, or be aligned with one another (Figs 1B and 7A). Published examples show symmetrical forms (Dżułyński & Walton, 1965; Anketell *et al.*, 1970; Fig. 7A and B), although they can also be asymmetrical (Fig. 7C). Whilst longitudinal ridges are occasionally utilized to derive palaeocurrent information (e.g. Basilici *et al.*, 2012; de Luca & Basilici, 2013; Dirnerová & Janočko, 2014), scales are rarely used in modern studies of turbidites (e.g. Dirnerová & Janočko, 2014), despite being known for more than six decades. However, in some cases scales may have been used but misidentified as flutes (e.g. Ricci Lucchi, 1995, plate 124; Boggs Jr, 2014, fig. 36; Dirnerová & Janočko, 2014, fig. 3D; Menzoul *et al.*, 2019), with the key differences that flutes do not stack in rows one upon another longitudinally (for example, Fig. 7A), do not show thin mud layers between their cuspate forms, and exhibit a characteristic three-dimensional morphology (Allen, 1971a).

Mechanisms

Experiments using plaster-of-Paris sediment gravity flows run over weakly consolidated clay beds (Dżułyński & Walton, 1965) have produced highly analogous structures to field examples of scales within longitudinal ridges and furrows (*cf.* Figs 8B and 7). These experimental patterns have been interpreted (Dżułyński &

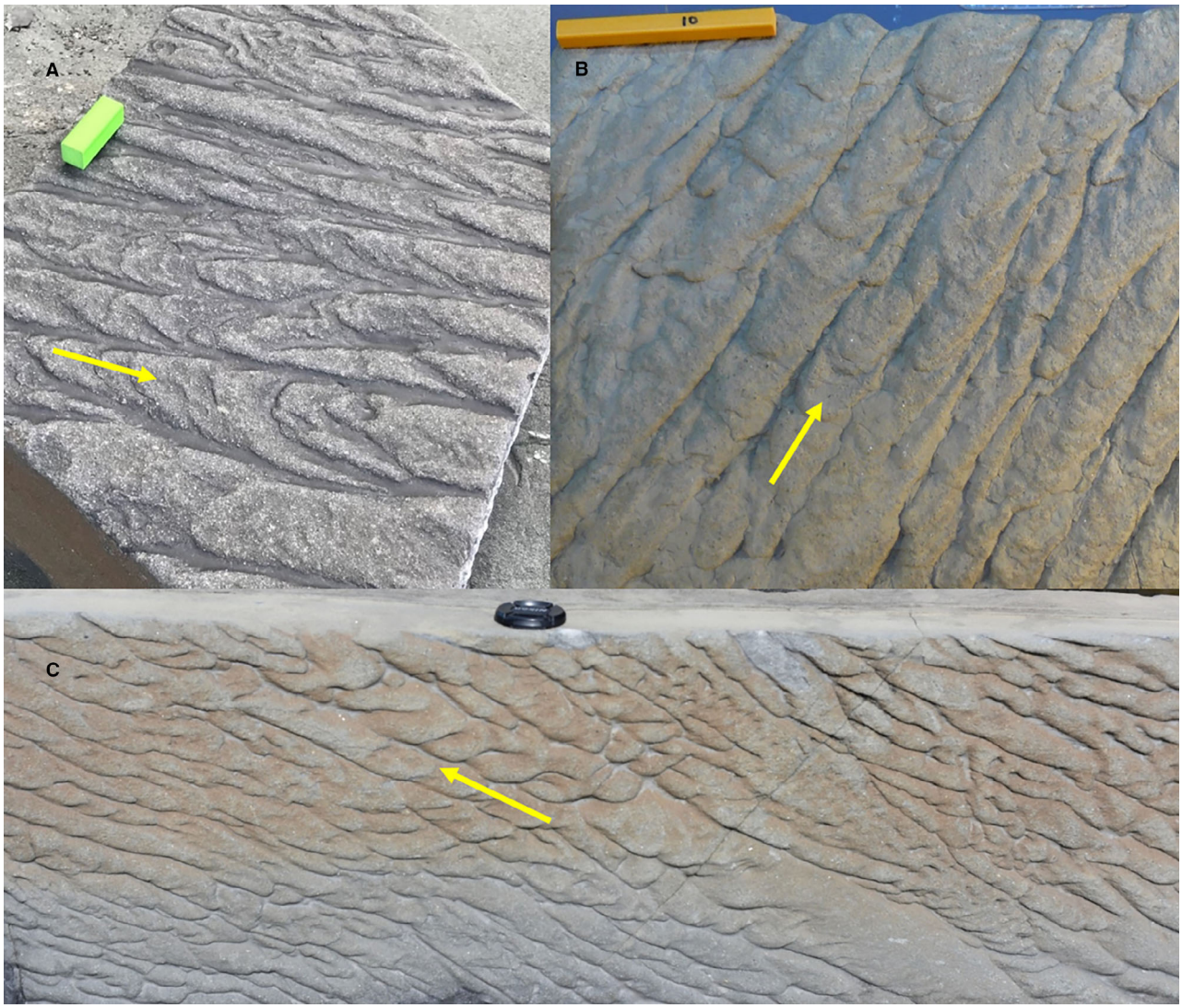

Fig. 7. Scales in longitudinal ridges and furrows. (A) Example showing scale morphology; flow to the right. Middle Ordovician Cloridorme Formation, Gaspé Peninsula, Quebec, Canada (See Model1). Scale bar is 50 mm long. (B) Scales and longitudinal ridges and furrows; flow to the top right. Oligocene, Cergowa Sandstone, Poland. From a sample in the collection of the Natural Sciences Education Centre at the Jagiellonian University, Kraków, Poland. Scale bar is 100 mm long. (C) Scales and longitudinal ridges and furrows in a near vertical outcrop, showing variability across the bedding plane. Flow to the top left. Middle Ordovician Cloridorme Formation, Gaspé Peninsula, Quebec, Canada. Lens cap for scale, diameter 77 mm. See also Model2 for a further example of extensive scales within longitudinal ridges and furrows. Yellow arrows give flow directions.

Simpson, 1966a, 1966b; Anketell *et al.*, 1970) in terms of ideas developed using heated plates to generate reversed density gradients in air, in the absence or presence of a horizontal shear (Graham, 1933). These experiments on instabilities in air flows showed that, in the absence of shear and with appreciable temperature differences, polygonal patterns are formed (Fig. 8A; Graham, 1933; Bodenschatz *et al.*, 2000). Where the less dense fluid is also more viscous, downward motion occurs in the centre of the polygons with upward motion at the edges (Graham, 1933; see also Anketell *et al.*, 1970, for sediments). The addition of a weak shear flow, in combination with buoyancy, leads to elongation of these structures, and the formation of cuspate forms that open downstream (Fig. 8A, section 'B'; Graham, 1933). With further increase in shear relative to buoyancy, the cusps (scales) are lost and longitudinal structures are formed (Graham, 1933). The scales observed in the plaster-of-Paris experiments were interpreted on this

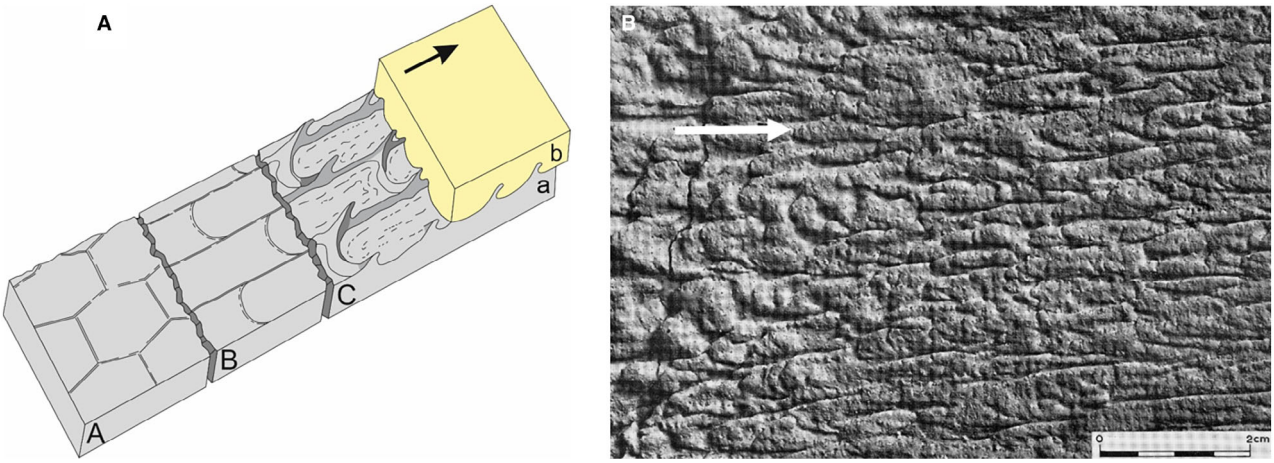

Fig. 8. (A) Schematic diagram for the formation of scales, showing flow 'b' with a density greater than the substrate 'a'. The combination of the density difference and flow shear leads to the curved surfaces in part 'C'. Longitudinal sector 'A' refers to the polygonal structure formed with a reversed density gradient in the absence of flow. In the polygons, downward motion occurs in the centre and upward motion at the edges (Graham, 1933). Sector 'B' refers to the longitudinal ridges and furrows produced through the addition of a flow (alongside buoyancy), here shown with scales, and section 'C' to the formation of facing 'cusps' pointing in the direction of shear. After Anketell *et al.* (1970). Note, that in other cases the polygons can be aligned, rather than offset, in planform (Graham, 1933; Anketell *et al.*, 1970) in which case scales can be found parallel to one another in adjacent furrows, rather than offset as shown in the present figure. (B) Longitudinal ridges and furrows with abundant scales, produced experimentally using plaster-of-Paris sediment gravity flows over clay beds (from Dżułyński & Walton, 1965, reproduced with permission of Elsevier); white arrow shows flow direction.

basis, with the muddy substrate assumed to have a greater kinematic viscosity but lower density than the overlying flow, leading to diapiric rise of the substrate at the edges of the cusps (Dżułyński & Simpson, 1966a, 1966b; Anketell *et al.*, 1970). In experiments that produced polygonal structures, the points where the hexagonal structures meet have diapiric structures that penetrate upward, and thus in the case of longitudinal ridges and furrows these diapiric structures are proposed to be higher where the cusps and longitudinal ridges meet (Fig. 8A; Anketell *et al.*, 1970). In turn, these structures are envisaged to start being deformed by the shear induced by the flow, causing them to point in the direction of shear (Anketell *et al.*, 1970). Graham (1933) showed that, depending on the initial deformation, the cusps can either form *en-echelon* (aligned with one another between adjacent furrows), or can be laterally offset from one another (Dżułyński & Simpson, 1966a, 1966b; Anketell *et al.*, 1970). Scales are thus interpreted to form under the influence of a weak shear flow, with the presence of a stronger shear flow leading to the formation of regular longitudinal ridges and furrows (Anketell *et al.*, 1970). Whilst a coherent theory underpins the model of Anketell *et al.* (1970), it is unclear how much evidence there is from sediment gravity flow experiments, other than the preserved structures on the soles of the plaster-of-Paris beds (Fig. 8B), because cross-sections from the experiments were not presented. Kuenen & Menard (1952) may have produced equivalent features in their experiments using dense particulate suspensions moving over clay beds, but they only show a cross-section of flame-like features (their fig. 6), with no planform data.

Similar features have been observed in deposits of the 2004 Indian Ocean tsunami (Matsumoto *et al.*, 2008), in the form of flames (20 to 60 mm high) that dip downflow and are cuspate in planform (50 to 100 mm in diameter), with the cusps opening downstream (Fig. 9; Matsumoto *et al.*, 2008). Observations from a series of trenches, in combination with 'opencast excavation', enabled the three-dimensional morphology of these structures to be reconstructed. These features were shown to be syn-sedimentary as they were truncated by parallel-laminated sands representing upper-stage plane beds (Matsumoto *et al.*, 2008). The full tsunami deposit formed from two waves, consistent with observations

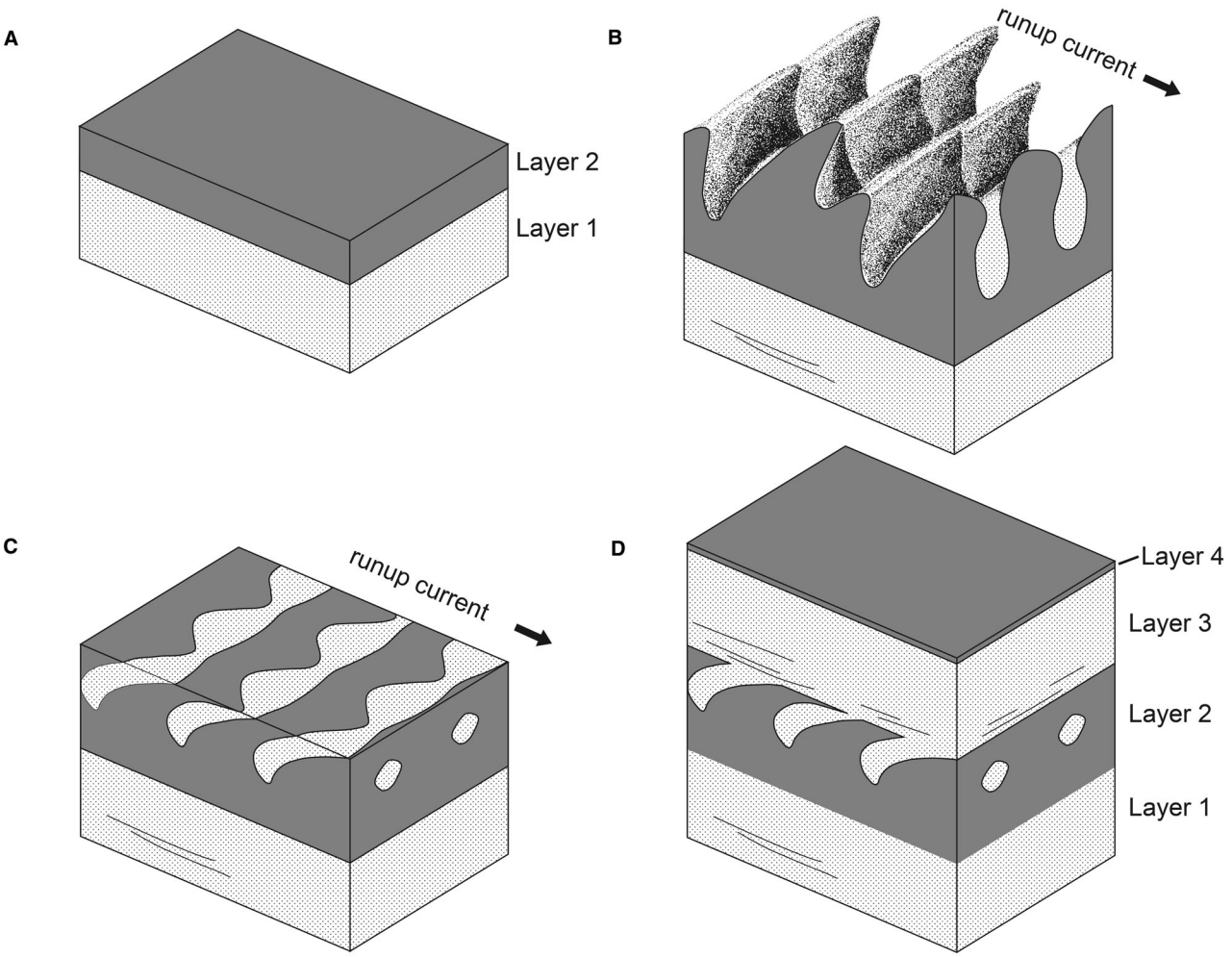

Fig. 9. Model for the formation of scale-like structures in the deposits of the 2004 Indian Ocean tsunami. (A) Initial sandy layer 1, and overlying muddier layer 2 that has undergone rapid suspension settling. (B) The second tsunami wave causes deformation of layer 2 to produce scale-like features. (C) Truncation of these structures then occurs, prior to (D) deposition of parallel-laminated sands on top of the structures. From Matsumoto *et al.* (2008) reproduced with permission of John Wiley & Sons Ltd.

from witnesses of two inundations. The upper part of the first deposit is mud-rich, fine-grained sand, with locally up to 3.6% mud, and was hypothesized to have settled from suspension prior to the arrival of the second wave (Fig. 9A; Matsumoto *et al.*, 2008). The second wave then induced deformation of this mud-rich layer, producing the scale-like structures, and their cleaner, coarser sand infill, prior to truncation by the same wave (Fig. 9B and C) and deposition of an overlying sand (Fig. 9D). Although Matsumoto *et al.* (2008) stated that: "this feature is not described from any known deformation structure", these structures are remarkably similar to the three-dimensional morphology of the scales reported by Anketell *et al.* (1970; Fig. 8A). Two models for the formation of these structures were proposed by Matsumoto *et al.* (2008): (i) shear stress influencing flame structures that formed under loading deformation; and (ii) shear-stress induced Kelvin-Helmholtz instabilities on the interface of the substrate and the overlying current.

Discussion of mechanisms

Scales are postulated to be generated as a result of a relatively weak shear flow interacting with buoyancy-induced diapirism of the underlying substrate into the overriding and denser flow (Dżułyński & Simpson, 1966a, 1966b; Anketell *et al.*, 1970). Thus, scales form under flows with a weaker shear flow component than flows

generating longitudinal ridges and furrows (Dżułyński & Simpson, 1966a, 1966b; Anketell *et al.*, 1970). The experiments of Anketell *et al.* (1970) also suggested that, for the scales to form, the substrate requires a higher kinematic viscosity and lower density than the overlying flow, also similar to the requirement for longitudinal ridges and furrows. Yet, for the case of mud-rich flows, viscosity might be expected to be proportional to density and thus scales would not be expected to form. However, later work has indicated that for buoyancy-driven deformation with narrow diapiric structures, such as scales, the relationship proposed by Anketell *et al.* (1970) is typically not the case, and that substrate viscosity can be lower than that of the denser upper layer (Harrison & Maltman, 2003; Owen, 2003). The full role of viscosity in buoyancy-induced deformation remains an area to be explored (Harrison & Maltman, 2003). In both the experiments of Graham (1933) and the model of Anketell *et al.* (1970), there should be one scale per initial polygon, and thus scale spacing should be a function of polygon, and therefore furrow, width. However, in some cases (for example, Fig. 7A) the scale spacing is much shorter than its width, raising questions about the detailed dynamics that underpin this model; a revised model is required to explain this spacing. Asymmetrical scales, as reported herein for the first time (Fig. 7C), are postulated to be the product of changing flow directions during the flow. The example given herein is from the Cloridorme Formation, eastern Canada (Fig. 7C), where research has revealed variability in flow directions within single event beds (Parkash & Middleton, 1970; Pickering & Hiscott, 1985; Edwards *et al.*, 1994).

An alternative model for the development of scales has been proposed. This model suggested that scales form as a result of interference of transverse wrinkles with longitudinal ridges (Dżułyński & Simpson, 1966b). However, this model was not supported by the experiments undertaken by Dżułyński & Simpson (1966b), nor by subsequent work (e.g. Dżułyński & Simpson, 1966a; Anketell *et al.*, 1970). Consequently, this idea lacks any supporting evidence, in contrast to the evidence for a model based on combined buoyancy and shear. Furthermore, transverse wrinkles appear to be rare, in marked contrast to the ubiquity of longitudinal ridges and furrows (see *Transverse wrinkles* section), further suggesting that this is an unlikely model for the formation of scales.

One of the mechanisms proposed for tsunami-generated cuspate structures is similar to the buoyancy-induced and shear-induced model suggested for scales, with shear stress postulated to influence flame structures that formed under loading deformation (Matsumoto *et al.*, 2008). However, this proposed mechanism does not explicitly recognize a buoyancy force, with the inference being that the base of the tsunami flow was denser than the substrate, as has been inferred in other examples (Hill *et al.*, 2023). The cuspate tsunami-generated structures are located towards the maximum inland extent of the tsunami deposit (Matsumoto *et al.*, 2008) and are thus compatible with a relatively low flow velocity and shear at the location of these structures. A second model for the formation of these cuspate tsunami structures infers formation of Kelvin-Helmholtz instabilities at the sediment interface. Kelvin-Helmholtz instabilities are widely recognized in sediment gravity flows (e.g. Simpson, 1997; Kostaschuk *et al.*, 2018), and have also been inferred within sediment layers with density differences across them, triggered by earthquake shaking (Heifetz *et al.*, 2005). However, Kelvin-Helmholtz waves in a rapidly moving flow are dynamic, rather than fixed (e.g. Kostaschuk *et al.*, 2018), and thus should propagate across the surface rather than stabilize in fixed positions (*cf.* Heifetz *et al.*, 2005). Consequently, such a Kelvin-Helmholtz instability mechanism is considered untenable herein. Therefore, these tsunami-induced cuspate structures are interpreted to form via a combination of buoyancy and shear in the same way as scales.

Transverse wrinkles

Characteristics

Transverse wrinkles (*sensu* Dżułyński & Sanders, 1962) possess millimetric widths and crestlines orthogonal to the flow direction (Figs 1C and 10). The wrinkles may be symmetrical or asymmetrical in cross-section (either upstream or downstream; Fig. 10; Dżułyński & Walton, 1965, fig. 89) and appear to be rare, recorded in just a few examples (Dżułyński & Sanders, 1962; Dżułyński & Walton, 1965; Dżułyński & Simpson, 1966a; Daly, 1968; Allen, 1971a). These features that occur on the soles of sandstone beds should not be confused with physically-induced or microbially-induced 'wrinkle structures' that are preserved on the tops of beds (e.g. Reineck, 1969; Allen, 1985a;

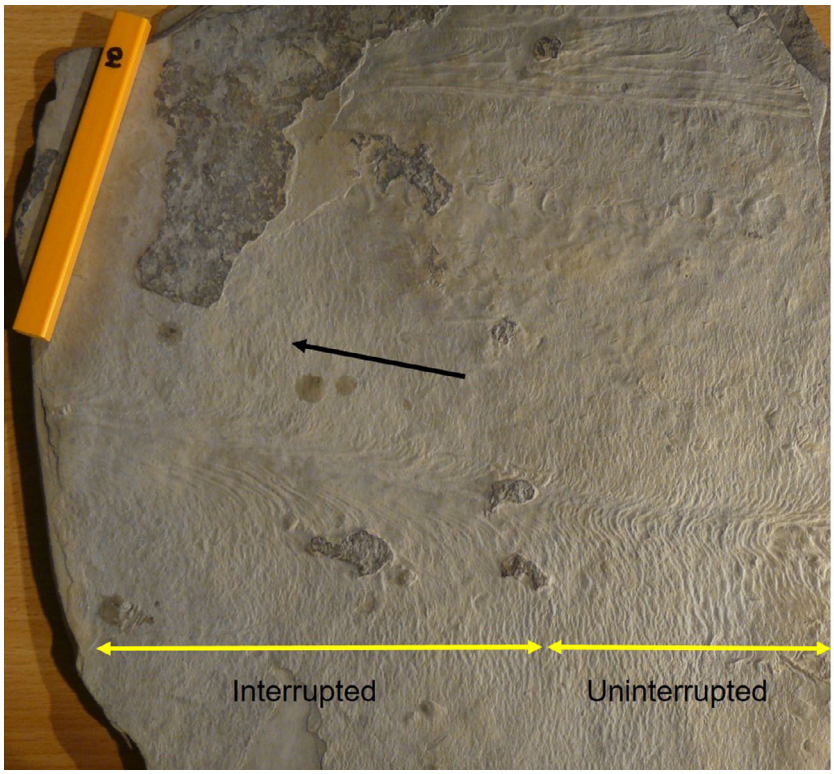

Fig. 10. Transverse wrinkles on the sole of a sandstone bed, later deformed to produce uninterrupted and interrupted chevron marks (as shown by the yellow arrows); flow direction shown by black arrow. Oligocene, Krosno beds, Poland. From a sample in the collection of the Natural Sciences Education Centre at the Jagiellonian University, Kraków, Poland. Yellow scale bar is 100 mm long.

Porada & Bouougri, 2007; Davies *et al.*, 2016; Wignall *et al.*, 2020).

Formative mechanisms

Dżułyński & Sanders (1962) linked the formation of transverse wrinkles to direct shear-induced deformation by a flow acting on a weak substrate, and consequently placed them in a separate category of 'deformation caused by currents', alongside scour mark and tool mark categories (Dżułyński & Sanders, 1962; Dżułyński & Walton, 1965). It was subsequently suggested that the interference of transverse wrinkles with longitudinal ridges led to the formation of 'scales' (Dżułyński & Simpson, 1966b; see discussion in the *Scales* section). An experimental example of transverse wrinkles was claimed from plaster-of-Paris flows over muddy substrates (Dżułyński & Simpson, 1966a, citing Dżułyński & Walton, 1965, fig. 138). However, these structures are laterally discontinuous and were referred to as transverse scours by Dżułyński & Walton (1965). Experiments with open-channel clear-water flows over soft mud beds also showed some millimetric wrinkles, transverse to flow, on a few examples (Allen, 1971a, fig. 106). However, Allen (1971a) linked these structures to shearing surfaces a few millimetres deep, and thus postulated that they were tensional features, an argument also favoured for the field examples studied by Daly (1968).

Polygonal, scaly and longitudinal ridges and furrows on mud ripples

Characteristics

Mud ripples are asymmetrical transverse structures in muds that resemble ripples with low-angle stoss sides and steeper, shorter, lee sides (Figs 1D and 11). They are preserved through infill by overlying sands, and therefore are seen as sole structures on the base of sand beds. Mud-ripple wavelengths range from 0.02 to 0.40 m, but exhibit uniform wavelengths within individual ripple sets (Fig. 11; Allen, 1982). Mud ripples can either have smooth surfaces (with or without small discontinuous tool marks), or part or all of the ripples can be covered in smaller deformational structures. These typically consist of polygonal patterns on lee slopes and in troughs, short cuspate features on the lower stoss slope, and more elongate features with crescentic heads higher up the stoss slopes (Figs 1D and 11). These cuspate features on the lower and upper stoss slope typically show analogies with scales, and longitudinal ridges and furrows, respectively (Figs 1D, 11A and 11B). The flaring of the heads

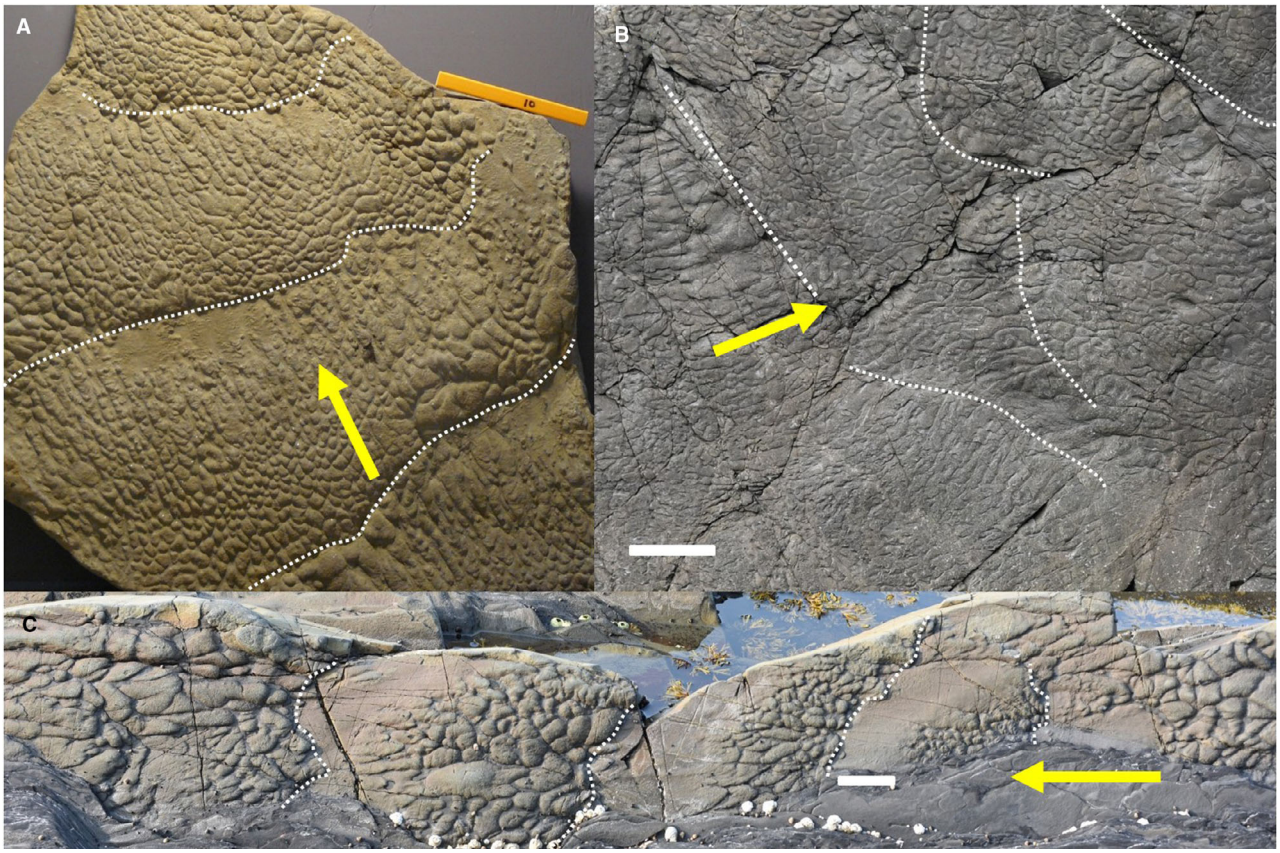

Fig. 11. Examples of mud ripples with polygonal structures and scaly longitudinal-furrow like structures. Yellow arrows point down current. White dotted lines show crestlines separating stoss and lee sides of bedforms. (A) Mud ripples showing polygonal structures in the lee and troughs of ripples, and longitudinal-furrow like features on the stoss sides. Krosno beds, Oligocene, Poland. From a sample in the collection of the Natural Sciences Education Centre at the Jagiellonian University, Kraków, Poland. Yellow scale bar is 100 mm long. (B) Three-dimensional, low relief mud ripples, with dominantly polygonal structures ('dinosaur leather'). The yellow arrow gives an overall flow direction, but the structures indicate that the flow patterns are more three-dimensional. Carboniferous Crackington Formation, North Devon, UK. White bar for scale, 150 mm. (C) Mud ripples with deeply indented polygonal structures, with furrow-like structures decreasing in amplitude up the stoss sides, and stoss crests that are planar. Middle Ordovician Cloridorme Formation, Gaspé Peninsula, Quebec, Canada. White bar for scale, 80 mm. See also Model3. An example of a large bedding plane with extensive scaly and polygonal structures ('dinosaur leather') is shown in Model4. A line drawing showing the different morphologies is shown in Fig. 1D.

of the furrows and scales match the direction obtained from the asymmetry of the mud ripples, and therefore open in the direction of flow. The term 'dinosaur leather' has been used for cases where these polygonal and scaly structures cover the entire surface of the mud ripples (Fig. 11A and B; Chadwick, 1948; Dżułyński & Simpson, 1966a). The formation of mud ripples has been linked to 'fluid-stressing' of weak mud beds by strong currents, with 'fluid-stressing' defined as erosion by a fluid without particles, and thus where abrasion by particles is not a factor (Allen, 1971a, 1982). However, the more detailed processes of erosion, or potentially shear-induced deformation of the bed, involved in the generation of mud ripples are unclear (Allen, 1971a). Herein, the focus is on the formation of the smaller structures that ornament the surfaces of the mud ripples.

Formative mechanism: turbulent vortices impinging on soft muds

Experiments with clear water open-channel flows

Experiments with water flows over mud beds have produced mud ripples that varied from

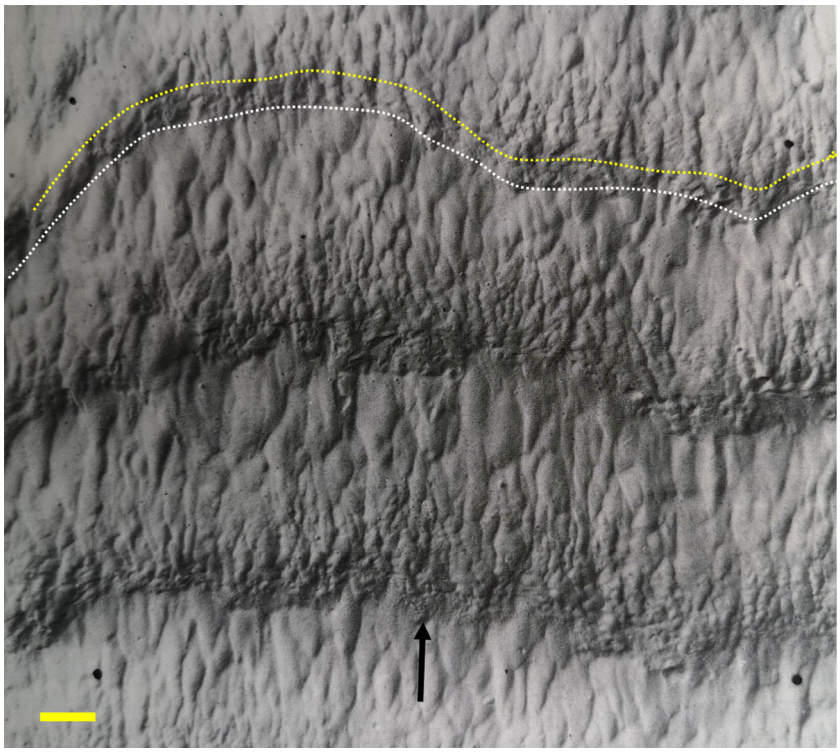

Fig. 12. Plaster-of-Paris mould of mud ripples formed in weak mud beds. Duration of the open-channel flow was 39.8 s, and the flow had a mean velocity of *ca* 0.55 m s^{-1}, and a flow depth of *ca* 78 mm. Black arrow shows flow direction, crest line of the mud ripple at the top of the image shown by white dotted line, and base of lee slope by yellow dotted line (modified from Allen, 1982, photograph reproduced with permission of Elsevier). The yellow scale bar is 10 mm.

smooth surfaces to complete coverage by small-scale structures, depending on flow and substrate conditions (Fig. 12; Allen, 1971a). Mud beds were composed of kaolinite–water mixtures, with some having bentonite as a component (2.5% of the clay fraction). This produced substrates with water contents of 64 to 71% (Allen, 1971a), equivalent to the stiff mud (≥10 years of consolidation) to hard mud (≥100 years of consolidation) classifications of van Rijn (1993), allowing for kaolinite as the dominant clay type in these experiments (see McGowan *et al.*, 2024, for discussion). However, the experimental setup of Allen (1971a) led to marked stratification within the substrates, with the upper parts of beds too weak to accurately measure shear strength using a shear vane tool, but not exceeding a shear strength of a few Pascals (Allen, 1971a). This is equivalent to a Bingham type fluid mud (≥ a week of consolidation) or potentially the lower end of the dense fluid mud (≥ a month of consolidation) category in the classification scheme of van Rijn (1993; see strengths tabulated in table 2 of McGowan *et al.*, 2024). The shear vane tool results therefore indicate that water contents in the experiments of Allen (1971a) can be highly misleading as an indicator of substrate strength (see earlier discussion in the *Longitudinal ridges and furrows* section).

Flow velocities reported by Allen (1971a), were *ca* 0.35 to 0.80 m s^{-1}, flow depths *ca* 20 to 110 mm and run times *ca* 20 to 250 s. The small-scale structures were termed polygonal and elongate marks by Allen (1971a), with the former forming in the troughs and lee of the ripples, and the latter on the stoss sides (Fig. 12). The elongate marks were ascribed to periodic turbulent flow events in areas where the boundary layer was attached. The brief nature of these turbulent events thus implies that these marks were rapidly modified or destroyed (Allen, 1971a). In contrast, the polygonal features were linked to the area of flow reattachment where downward impinging eddies altered the bed, with: "each depression the product of the interaction of a single eddy of flow with the mud bed" (Allen, 1971a).

Experiments with plaster-of-Paris density currents

Plaster-of-Paris density currents, similar to those discussed in the *Longitudinal ridges and furrows* section, were run over pre-formed topography (Dżułyński & Simpson, 1966a, 1966b). A series of sand ripples were built in the laboratory, and then covered by clay settled from suspension (Dżułyński & Simpson, 1966a). The plaster-of-Paris flows, representative of dense flows of *ca*

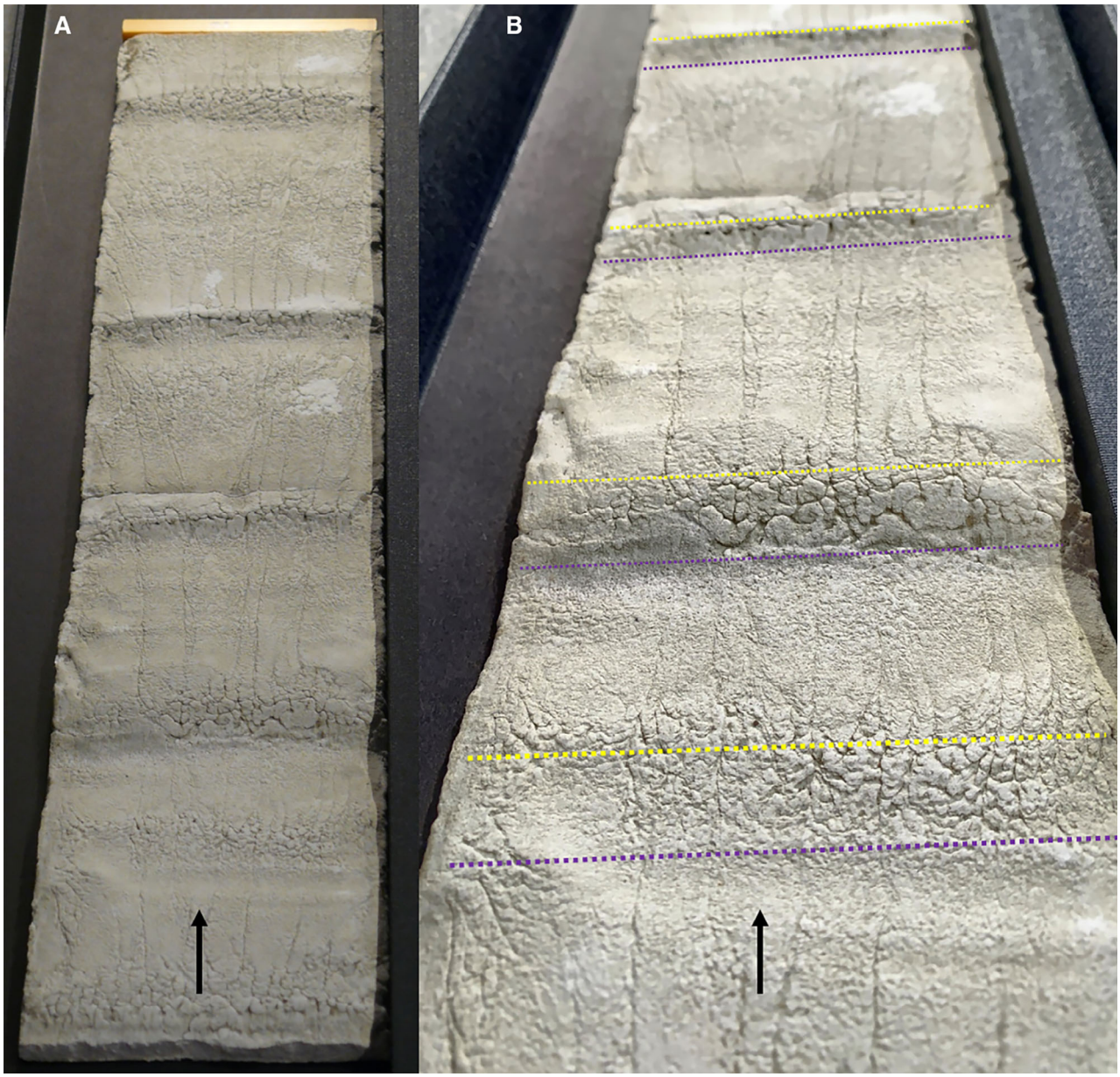

Fig. 13. Images of plaster-of-Paris moulds of experimental mud ripples, with small-scale structures in the troughs and on the lowermost part of the stoss side. (A) Series of mud ripples. Black arrows show flow direction. Yellow scale bar is 100 mm long. (B) Close up of ornamentation on the experimental mud ripples, showing equant structures in the lee and the trough of the ripple, with these structures becoming more elongate on the lowermost parts of the stoss slope. Crest lines shown by purple dotted lines, and base of lee slope by yellow dotted lines. Note that, as this is a mould, the structures are all inverted. From samples in the collection of the Natural Sciences Education Centre at the Jagiellonian University, Kraków, Poland. The experiments are reported in Dżułyński & Simpson (1966a, 1966b) and presented in Dżułyński (2001).

1260 to 1520 kg m^{-3}, and analogous to transitional plug flows (*sensu* Baas *et al.*, 2009) or intermediate-strength debris flows (*sensu* Talling, 2013), were then run over this topography for tens of seconds to possibly several minutes (see *Longitudinal ridges and furrows* section). These produced more equant, polygonal deformation in the lee and trough of the bedforms, and slightly more elongate scale-type features on the lowermost parts of the stoss side (Fig. 13). The edges of these structures are better defined, without the obvious erosion and overprinting

(*cf.* Figs 12 and 13) seen in the open-channel experiments of Allen (1971a). The experiments were interpreted in a similar way to Allen (1971a), with polygonal patterns linked to the formation of turbulent vortices in the lee of the ripple crests (Dżułyński & Simpson, 1966b; Dżułyński, 1996).

Discussion of mechanisms

The small-scale structures developed in the experiments of Allen (1971a) bear a superficial resemblance to those in natural examples, although they are the product of multiple structures that constantly modify and rework one another. Consequently, there are many overlapping structures and remnants of structures, and individual structures exhibit complex boundaries (Fig. 12). This is in contrast to those in natural systems that show a much higher degree of alignment between the elongate structures, with clearer and simpler boundaries (Figs 1D and 11). Similarly, the polygonal patterns are again more distinct, uniform and polygonal in natural examples (Fig. 11). The plaster-of-Paris flows over pre-formed mud-ripple topography produced equant, polygonal features and scaly structures (Fig. 13) that are much better defined than those in the experiments of Allen (1971a), and more analogous to those formed in natural systems. However, the interpretation of each polygon or scale being formed by individual vortices in the plaster-of-Paris experiments appears problematic, as the lack of cross-cutting suggests that the vortex positions were constant, which is not a property of turbulent flows. Furthermore, the dense nature of the plaster-of-Paris flows, and their viscosity of around 1.0 to 2.5 Pa s^{-1} — comparable to runny honey (Yanniotis *et al.*, 2006; Peakall *et al.*, 2020) and around three orders of magnitude greater than water — suggests that turbulence should be less important in these experiments relative to the clear water flows of Allen (1971a).

An alternative explanation is that these experimental structures were also strongly related to the reversed density gradient between the underlying substrate and the denser plaster-of-Paris flows, as also implied herein for longitudinal ridges and furrows, and scales. However, this aspect is largely unremarked upon in the original experiments of Dżułyński & Simpson (1966a, 1966b) and Dżułyński (1996). The theory outlined above for the formation of scales suggests that polygonal structures form in areas with density inversion but no significant flow, and thus where buoyancy-driven forces dominate. In contrast, scales form in areas with weak flow relative to buoyancy, and longitudinal ridges and furrows form in areas where flow shear is stronger. Such a theory fits the known distribution of flow over ripples (e.g. Baas & Best, 2008), with low velocities in the separation or expansion zone in the lee of the ripple, and velocities increasing up the stoss side (Fig. 1D). Thus, polygonal or equant forms are found in the lee and trough, and scales are found on the lowermost parts of the stoss side (Fig. 1D). The absence of longer scales on the rest of the stoss side, as observed in some natural examples (Figs 1D, 11A and 11B), may reflect erosion of the muddy material from the upper parts of the stoss side, and accumulation of this sediment in the troughs. This contention is supported by the depth of structures being greatest in the troughs and decreasing and finally terminating along the stoss side, as often seen in natural examples (Fig. 11C).

Irregular orientated and non-orientated structures

Characteristics

Alongside the structures described previously, there is also a range of structures that do not easily fit into the existing categories. These range from 'non-orientated irregular dimpled structures' (see page 79 of Dżułyński & Walton, 1965), to short and partially irregular structures that exhibit an overall linear fabric (Fig. 14). In some of these examples, there can be considerable variation in the size and orientation of structures within a small area (Figs 14 and 16).

Formative mechanisms

Some of these structures, such as those in Fig. 14, have been identified as load casts, but classical load casts occur by gravitational loading of an unstable system (a Rayleigh–Taylor instability: denser layer above less dense), typically in the absence of a flow (Dżułyński & Walton, 1963; Allen, 1982; see discussion in *Differentiating FIDS from load casts and flames* below). Consequently, the preferred orientation of the structures is difficult to explain through purely vertical gravitational loading (Fig. 14). The smaller structures visible in Fig. 14A are also cut by the skim marks, and thus were formed earlier, with the skim marks also broadly aligned with the smaller structures. Skim marks themselves are formed by a flow with considerable cohesive strength, but in which tools can arc down, and

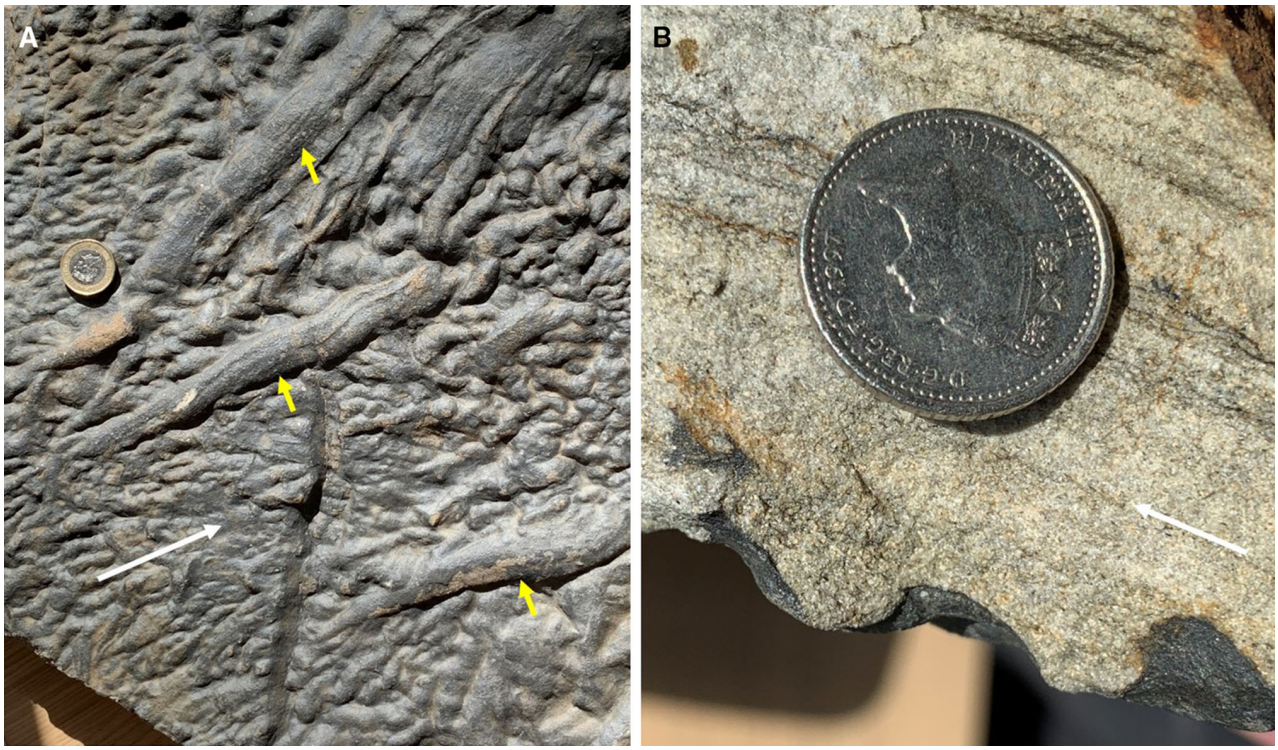

Fig. 14. (A) Short, elongate, structures displaying a dominant orientation, albeit with considerable variation, on the sole of a turbidite bed. These structures are cut by skim marks (yellow arrows), most of which are in the same orientation. The skim marks themselves exhibit deformed margins. White arrow shows flow direction. Coin for scale, 23.4 mm in diameter. (B) Cross-section showing faint planar lamination in overlying sands, infilling the undular FIDS surface. This section is located just beyond the top left hand corner of the slab shown in part A, and is orientated approximately 10° from the longitudinal direction of the FIDS. This is taken from a counterpart slab; flow direction is from right to left. Coin for scale, 24.5 mm in diameter. Both examples from Pendle Grit, Carboniferous, Wiswell, Lancashire, UK.

then away, from the bed (Peakall *et al.*, 2020). Here, the skim marks exhibit crenulated edges, reflecting deformation of their sides, suggesting that the substrate was still relatively weak at the time of their formation. Thus, these cross-cutting relationships, and the similarities in orientation of the smaller-scale structures and the skim marks, indicate that the smaller orientated structures formed in a relatively weak mud bed *prior* to the deposition of the overlying sand bed, thus suggesting that they may be flow-related. When seen in cross-section (Figs 14B and 15), the structures are filled by dominantly planar laminated sands, suggesting that there must have been substrate topography that had formed prior to deposition. Importantly, subsequent loading of the substrate is either minor or has not occurred at all (Figs 14B and 15). Figure 16 shows irregular orientated and non-orientated structures in patches, separated by small-scale longitudinal ridges and furrows. It is unclear whether this is the product of small-scale variations in flow velocity, with non-aligned areas representing slower zones, and ridges and furrows representing faster zones, as argued by Dżułyński (2001).

DISCUSSION

Sedimentary structures: overview and problems

The sedimentary structures produced in the experiments of Dżułyński and co-workers (e.g. Dżułyński, 1965, 2001; Dżułyński & Walton, 1965; Dżułyński & Simpson, 1966a, 1966b) are remarkably analogous to natural examples of longitudinal ridges and furrows, scales, and polygonal and scaly structures over mud ripples. This contrasts with the experiments of Allen (1969, 1971a) for small-scale structures formed across mud ripples, and longitudinal ridges and furrows, which bear some superficial similarities, but are not strongly analogous to natural

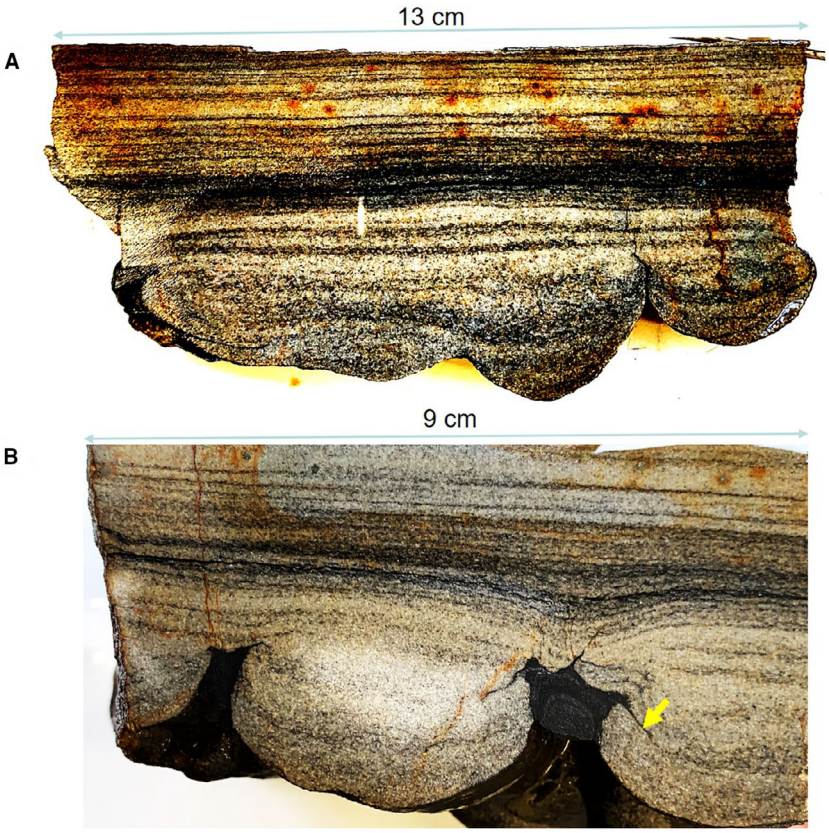

Fig. 15. Cross-sections through FIDS from a single block of the Pendle Grit Formation from the same bed seen in Fig. 14A. (A) A cross-section at an angle of *ca* 40° to FIDS elongation (actual down-flow direction unclear). (B) The example is orthogonal to the elongation direction and shows cross-sections of elongate ridges and furrows. Infill in (A) and (B) is dominantly planar laminated but shows initial healing of the topography (in B), with beds thickening into low-points. Post-depositional features include the slight concave inflection of the bedding planes at the margins of the FIDS, caused by minor loading, and millimetre-scale mud injection veins (example arrowed). Note that images have had their contrast enhanced.

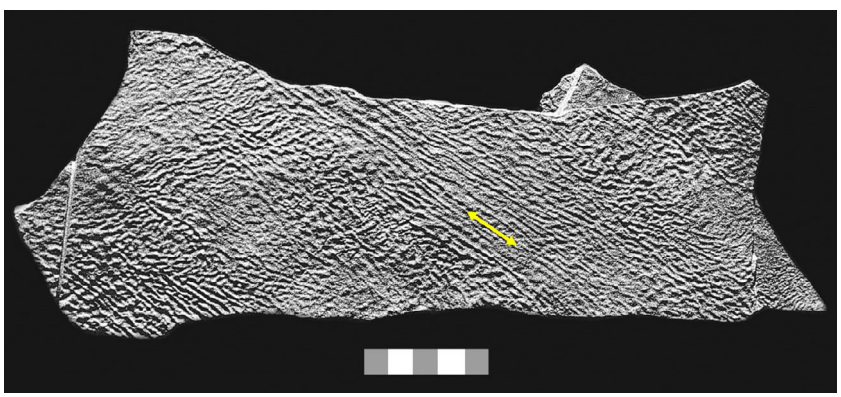

Fig. 16. Irregular orientated and non-orientated structures, in association with small-scale examples of longitudinal ridges and furrows. Krosno beds, Oligocene, Poland. Yellow arrow shows bidirectional flow direction. Scale bar is 50 mm broken into 10 mm increments (based on Dżułyński, 2001). Courtesy of Waldemar Obcowski. From samples in the collection of the Natural Sciences Education Centre at the Jagiellonian University, Kraków, Poland.

examples. Other structures, such as those in the irregular orientated and non-orientated structures category, have received less attention in terms of their formative mechanisms. Yet, the structures generated in the experiments of Dżułyński and co-workers are interpreted in a variety of ways. Scales were dominantly related to reversed density gradients between the flow and the bed, interacting with a shear flow, whilst longitudinal ridges and furrows were dominantly linked to helicoidal flows that cause scour, and induce deformation via lateral shear drag normal to the flow. Lastly, polygonal features associated with mud ripples were interpreted in terms of

turbulent vortices impinging on soft muds. The wide range of processes invoked for the same experiments, and the attribution of specific processes to individual sedimentary structures, renders their interpretation strikingly complicated. This is particularly true in comparison to process models of sedimentary structures such as aggradational bedforms in sand, and erosional sole structures in deep-marine systems (e.g. Baas *et al.*, 2016a, 2021a; Peakall *et al.*, 2020), which demonstrate a wide range of depositional and erosional bedforms generated through progressive changes in flow rheology and substrate character. Herein, a new holistic model is proposed for the formation of the structures documented above.

Flow-induced interfacial deformation structures (FIDS)

Two key observations are present in the seminal experiments of Dżułyński and co-workers. Firstly, the structures formed quickly (in tens of seconds to perhaps 1 to 2 min) and thus there was little time for scour, in keeping with the lack of evidence for scour structures and erosional products. Secondly, the plaster-of-Paris flows were much denser (*ca* 1260 to 1520 kg m^{-3}) than the substrate (*ca* 1050 to 1150 kg m^{-3}), and thus considerable buoyancy forces were present in the experiments. Given these observations, and the physical theory of Anketell *et al.* (1970), it is proposed that these structures can be explained as what are herein termed flow-induced interfacial deformation structures (FIDS). In these FIDS, the soft cohesive substrate undergoes deformation in response to a buoyant force induced by the denser basal component of an overriding flow, and the flow interacts with this buoyant deformation through shear to remould the substrate.

The relative strength of these buoyant and shear-induced forces explains the wide range of sole structures — FIDS — that can be formed. In areas such as the recirculation zone in the lee of mud ripples, where shear forces are limited, buoyancy forces lead to purely vertical deformation, and the production of polygonal structures (Fig. 1D). The addition of a small amount of shear along the ripple stoss side deforms these buoyancy-induced polygons and leads to the formation of scales, within longitudinal ridges and furrows, on the lowermost parts of the stoss side of the mud ripples. As shear forces increase further, relative to the buoyancy forces, the scales are lost, and regular longitudinal ridges and furrows are formed.

Such an interpretation is reinforced by the observations of irregular orientated structures (Fig. 14), which indicate that substrate deformation occurred early, prior to the production of basal sole structures, and that the deformation also occurred prior to significant sedimentation. Furthermore, once deposition occurs then remoulding of the diapiric features will rapidly stop. Instead, deposition in the furrows would lead to an increased loading force. However, given the vertical length scales of these structures, the additional thickness of sand in the furrows relative to the ridges will likely result in very limited additional loading (for example, Figs 14B and 15). Thus, any lamination present within the furrows, would not be expected to be significantly deformed, as seen in the examples in Fig. 15. Considering this evidence, and the associated arguments, collectively, supports the presence of buoyancy-induced diapirism of the bed whilst a flow was running over the substrate, with sedimentation infilling the resultant topography during subsequent flow deceleration.

Flow-induced interfacial deformation provides a coherent process model that explains all of the sedimentary structures formed in the experiments of Dżułyński and co-workers, as a balance between buoyancy-induced forces and shear forces (Fig. 17). The short length of individual ridges and furrows, their variable width and sinuosity, and in some cases observations of a series of bulbous protrusions along their length, are in keeping with structures with a strong component of buoyancy-induced diapirism (Fig. 17A), as in mud and salt diapirs (e.g. Hudec & Jackson, 2007; Blanchard *et al.*, 2019). Scales also show a significant diapiric component. Furthermore, this model provides a coherent explanation for the distribution of structures across mud ripples (Fig. 17B). More irregularly orientated and non-orientated structures with spatial variability (for example, Figs 14 and 16) may reflect either local changes in substrate properties, small-scale temporal or spatial variability in the flows (e.g. Parkash & Middleton, 1970; Dżułyński, 2001), or potentially more complex interactions between buoyancy and shear forces (see comparison with fluid dynamics experiments below).

Transverse wrinkles

Transverse wrinkles have been linked to direct shear-induced deformation by flow on a weak substrate (Dżułyński & Sanders, 1962; Dżułyński

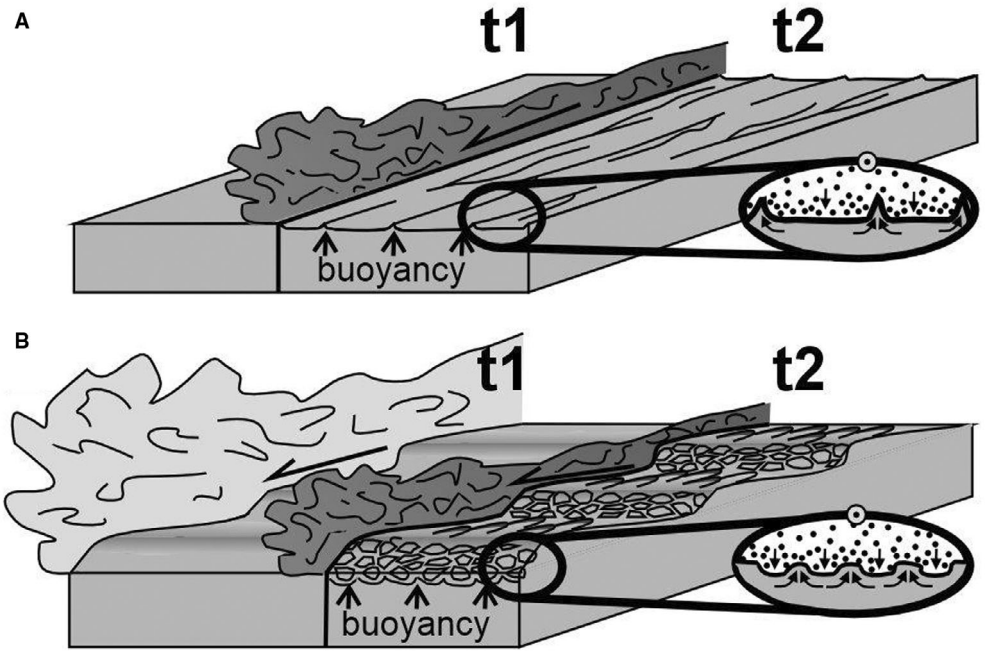

Fig. 17. Schematic process model for the formation of FIDS. (A) Initial weak muddy substrate (t1) that then undergoes deformation as a result of a high-density flow (t2). At t2, buoyancy forces lead to the growth of diapiric structures in the mud, with corresponding downward movement of the high-concentration flow. Subsequent deposition of sands leads to the formation of longitudinal ridges and furrows. (B) Low-density flow forming mud ripples (t1), followed in the same event by a higher-density flow that leads to the formation of FIDS on the surface of the mud-ripples (t2). More equant FIDS occur in low-velocity regions in the lee sides and ripple troughs (see inset for processes), whilst scale-like structures form on the stoss sides (t2). Insets also show downstream flow coming out of the page, as shown by the arrow head in the circle at the top.

& Walton, 1965). In this scenario, buoyancy plays either no role, or a very limited role, and shear is dominant. In this respect, transverse wrinkles are at the other end of the process spectrum to polygonal structures that are purely buoyancy-driven. As noted earlier, transverse wrinkles may also potentially be the product of other processes, such as tensional stresses within the substrate.

Comparison between FIDS, Rayleigh-Bénard convection (RBC) and inclined layer convection (ILC)

Comparisons can be made between FIDS, and their postulated control by the relative effects of buoyancy and shear forces, with Rayleigh-Bénard convection (RBC) and inclined layer convection (ILC). RBC is exemplified in a fluid, normally air in experiments, between two differentially heated horizontal closely-spaced parallel plates. The differential heating (heated from below and cooled from above) generates a reversed density gradient and the generation of instabilities in the fluid. If the differential heating across the plates is high, hexagonal forms are produced (Graham, 1933; Bodenschatz *et al.*, 2000). However, Graham (1933) also showed that the addition of a shear flow produces scales and longitudinal structures. More commonly, the interaction of buoyancy and shear forces is studied in ILC, where the inclination angle of the two closely spaced parallel plates is altered (e.g. Daniels *et al.*, 2000; Subramanian *et al.*, 2016). In this case, differential heating across the fluid leads to hotter, less dense fluid rising up the plate, and less hot, denser fluid flowing down, thus imposing a shear force. Numerical and experimental studies have focused on systems with small temperature differences that conform to the Oberbeck-Boussinesq approximation, in which density variations are assumed to be restricted to the buoyancy terms (Daniels *et al.*, 2000; Subramanian *et al.*, 2016). For low inclination angles, buoyancy dominates and longitudinal rolls are formed that are parallel to the shear flow, whilst at high inclination angles of 75 to 80° shear forces dominate and transverse rolls develop

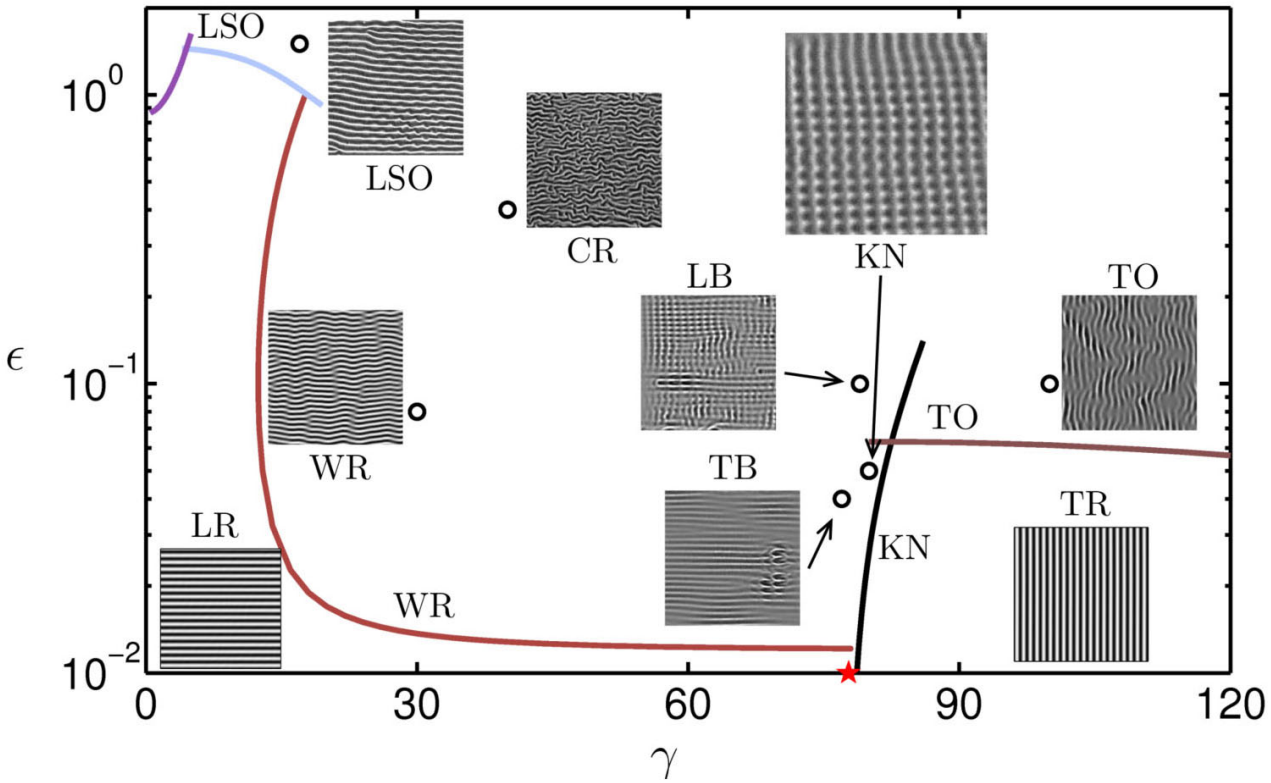

Fig. 18. Phase space of patterns produced by air in Inclined Layer Convection. γ is the inclination angle, and is a measure of the shear force, with values greater than 90° reflecting the whole double plate system overturning. ε is a dimensionless Rayleigh number, a measure, in part, of the buoyant force. Specifically, $\varepsilon = (R-R_c(\gamma))/R_c(\gamma)$ where R is the Rayleigh number, and $R_c(\gamma)$ is the critical Rayleigh number where periodic arrays of convection rolls initiate, which varies as a function of inclination angle. Furthermore, R is the ratio of buoyancy and thermal diffusivity. The red star represents the point where buoyancy and shear are equal. Points above the coloured lines represent secondary instabilities. The conditions assume a Prandtl number (the ratio of kinematic viscosity to thermal diffusivity) of 1.07, and therefore the momentum diffusivity and thermal diffusivity are approximately equal. CR, crawling rolls; KN, knot instability (image enlarged for clarity); LB, longitudinal bursts; LR, longitudinal rolls; LSO, longitudinal subharmonic oscillations; TB, transverse bursts; TO, transverse oscillations; TR, transverse rolls; WR, wavy rolls. Modified from Subramanian *et al.* (2016) incorporating shadowgraph generated images of experiments originally from Daniels *et al.* (2000).

(Fig. 18; Daniels *et al.*, 2000; Subramanian *et al.*, 2016). Beyond 90° there is a stable density gradient, and thus shear forces dominate. Secondary instabilities can also lead to a range of more complex patterns that have been widely studied as part of the field of pattern analysis (Fig. 18; Daniels *et al.*, 2000; Subramanian *et al.*, 2016, and references therein). Whilst these systems are relatively simple compared to FIDS, with a single fluid and the density difference being the product of heating, the broad trends in structures mirror those postulated herein for FIDS.

Longitudinal ridges and furrows are analogous to longitudinal rolls, wavy rolls and longitudinal subharmonic oscillations in the ILC system (Fig. 18), and thus form where buoyancy dominates over shear. In contrast, transverse wrinkles are analogous to transverse rolls and transverse oscillations with shear greater than buoyancy, and in many cases the product of pure shear. Irregular orientated and non-orientated structures are here postulated to be analogous to those structures that form where shear force and buoyancy are almost comparable (for example, knot instability, longitudinal bursts). However, FIDS are unlikely to exhibit perfect temporally steady flow as in an ILC system, and thus patterns likely lack such regularity. Although scales are not observed in the ILC system, they are observed experimentally at higher temperature gradients, under non-Oberbeck-Boussinesq conditions and low shear (Graham, 1933).

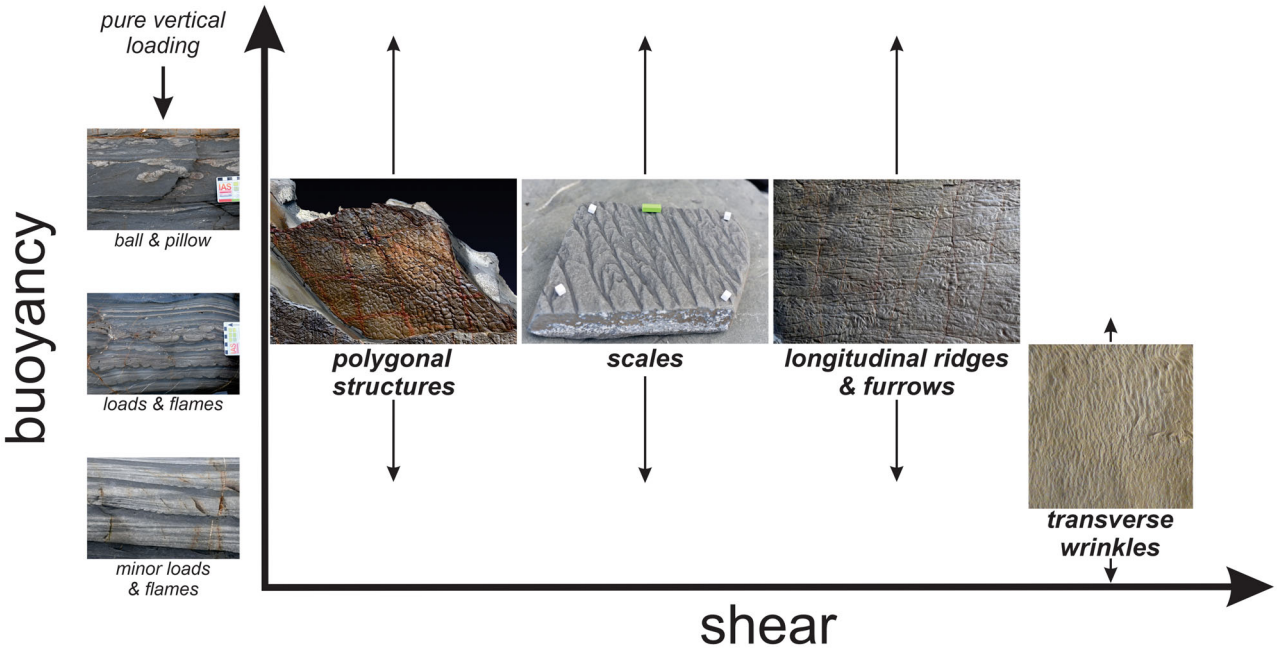

Fig. 19. Schematic phase space diagram of flow-induced interfacial deformation structures as a function of buoyancy and shear forces. Structures due solely to buoyancy and that occur post-deposition (flames, loads, balls and pillows) are shown on the left for reference. Note that this schematic diagram excludes consideration of the duration of deformation.

Although FIDS form in a more complex system, with a deforming lower density substrate, and a denser flow, each with different viscosities, the comparison with RBC and ILC reinforces the view that FIDS are the product of a dynamic interaction between buoyancy and shear forces. A schematic distribution of FIDS as a function of shear forces and buoyancy is illustrated in Fig. 19. It should be highlighted that time is not considered in Fig. 19, in part because the experiments of Dżułyński and co-workers demonstrate that the millimetric to tens of millimetric diapirism of FIDS can form very quickly, on the order of just a few minutes. However, an open question is whether the magnitude of the imposed forces, and their temporal duration, might have an influence on the nature of FIDS. The importance of this force magnitude and duration in boundary layers can be seen in the initiation of bedload transport in gravels, where impulse, the product of turbulent forces and their temporal duration, has been shown to be a key parameter (e.g. Diplas *et al.*, 2008). Future experiments may enable these schematic ranges to be refined, and for questions such as the influence of magnitude and duration to be examined.

Additional loading during, or after, sedimentation

Herein, the focus has been on the formation of structures as a function of buoyancy and shear forces. However, once sedimentation begins on these substrates, additional gravitational deformation may occur. Recently deposited muds, such as those involved in the formation of FIDS, exhibit plasticity, and will therefore flow if sedimentation leads to their yield strength being exceeded (Owen, 2003). The magnitude of loading is partly related to the thickness of the bed overlying the FIDS, along with the thickness and rheology of the mobile substrate. However, since the FIDS will have already partially, or fully, adjusted to the density contrast between substrate and flow, any additional loading will relate to the density difference between the formative flow of the FIDS, and the density of the final sedimented bed. Thus, herein it is postulated that most FIDS will not exhibit significant additional deformation (for example, Figs 14B and 15). However, some cases, such as the polygonal and scaly structures in mud ripples, can show bulbous forms that suggest additional loading during, or after, deposition (Fig. 11C).

Can FIDS form true substrates?

The concept that deposition occurs almost immediately behind the head of a density current, and thus sole structures are preserved almost instantly (Kuenen, 1957), has been an integral part of interpretations of the Bouma sequence (Bouma, 1962) and palaeohydraulic analyses of turbidites. However, this concept has been challenged recently, with evidence for a significant time gap between the formation of sole structures and overlying deposition from the same flow (Peakall *et al.*, 2020). Complete sediment bypass has also been argued to occur in some cases, with the sole structures and the overlying deposit being the product of different flows (Peakall *et al.*, 2020; Davies & Shillito, 2021; McGowan *et al.*, 2024). This allows the substrate to consolidate forming the 'true substrates' of Davies & Shillito (2021). Evidence also suggests that substrates cut by sole structures — such as grooves, chevrons and flutes — may form true substrates (Peakall *et al.*, 2020; Davies & Shillito, 2021; McGowan *et al.*, 2024). Formation of FIDS, however, occurs in weak substrates where the diapiric upward movement of less-dense substrate is balanced by downward movement of higher-density fluid from the overlying flow, and stabilization of these structures therefore requires rapid sedimentation in the same flow event. Consequently, FIDS are unlikely to act as true substrates. Furthermore, this suggests that where FIDS are cut by later sole structures, such as grooves and skim marks (see Fig. 14), this occurs within the same flow event.

Implications for flow dynamics

Flow characteristics

The presence of FIDS indicates that the formative flows are denser than the underlying substrate, and dense enough to trigger buoyancy-driven diapirism during the flow event. FIDS also show little evidence for scour, suggesting that the formative flows were non-erosive. Furthermore, the remoulding of the diapiric structures shows that a flow bypass phase can take place, indicating that the formative flow was not depositional during that phase. This lack of deposition is intrinsic to the buoyancy versus shear mechanism postulated for the origin of these structures. In addition, the basal part of the flow must also be sufficiently fluidal to flow between the growing diapiric structures, and thus basal conditions are incompatible with debris flows where the plug flow reaches all the way to the base (laminar plug flows, *sensu* Peakall *et al.*, 2020). This model of FIDS formation recognizes the importance of a flow bypass phase, and thus implies that the flow is not depositional upon arrival. Yet, shear at the base of sediment gravity flows can also act during deposition, through kinematic boundary layers (Butler *et al.*, 2016). However these kinematic boundary layers produce transverse-dominated structures in sands and muds, such as loads and flames, and inclined convolute lamination (Butler *et al.*, 2016). The dominance of diapiric forces in FIDS, their presence on mud ripples that were not deforming during the generation of FIDS, and the absence of transverse structures composed in part of deposited sands, all indicate that there was not significant shearing of the bed after the initiation of sedimentation. Therefore, there was an absence of a kinematic boundary layer.

The FIDS are therefore related to high-density flows that are initially bypassing and whose basal layer is fluidal; but, beyond this, what is the nature of these formative flows? High-concentration turbidity currents in a bypass phase, as observed in some laboratory experiments (Baker *et al.*, 2017), may be a possibility. Hindered settling as observed in high-concentration turbidity currents starts at concentrations of just a few percent by volume depending on grain size (Baas *et al.*, 2022), well below the widely used value of 10% (Bagnold, 1954). Conservatively, taking the 10% Bagnold value, flows only have densities of 1165 kg m^{-3}, assuming a density of 2650 kg m^{-3} for the sediment. If concentrations at the base approach the packing limit, perhaps 45 to 55% by volume, traction carpets may form (Hiscott, 1994), but these are not fully bypassing or sufficiently fluidal to be compatible with FIDS. High-concentration turbidity currents with basal concentrations between these two end members may potentially provide the requisite density difference, and the fluidal nature of the flow. However, as sediment concentrations rise in high-concentration turbidity currents, turbulence damping (Cantero *et al.*, 2012, 2014) may take place. If sediment concentrations become high enough for full turbulence extinction to occur, this may lead to rapid sedimentation (Cantero *et al.*, 2012), which is incompatible with the need for a sediment bypass phase as required for FIDS formation. Alternatively, the incorporation of mud into a sediment gravity flow leads to transitional flows (Baas *et al.*, 2009, 2011),

known to form a range of high-density plug flows at higher sediment concentrations. A fluidal basal layer is formed beneath these plug flows, the lowermost part of which is a thickened viscous sub-layer that may be of the order of 100 mm in thickness in natural flows (Baas & Best, 2002; Baas *et al.*, 2009, 2016a; Peakall *et al.*, 2020). These laminar basal layers are fluidal and high-density, but do not scour the bed (Baas *et al.*, 2009; Peakall *et al.*, 2020; McGowan *et al.*, 2024). Such flows may also account for the pristine preservation of FIDS, shielding the bed from turbulence and erosion, prior to sand deposition (see discussion in McGowan *et al.*, 2024, regarding the preservation of delicate chevron marks).

Flow transformation

The FIDS that ornament mud ripples likely formed in the same flow event as the mud ripples, because flow fields are observed to be in phase with the bedforms (i.e. the polygonal structures form in the lee and trough, scales are present in the lowermost part of the stoss side, and furrows form further up the stoss side – see *Polygonal, scaly and longitudinal ridges and furrows on mud ripples* above). Furthermore, more pronounced FIDS form in the trough whilst FIDS are absent or less pronounced on the upper stoss, suggesting that soft muds preferentially accumulated in the troughs, and there was little time for compaction. Similarly, the mud ripple substrate remains weak enough to undergo flow-induced interfacial deformation. Consequently, mud ripple formation by a fully bypassing current, followed rapidly by FIDS formation during a second event that exhibited flow characteristics in phase with the bedforms, appears improbable. However, whilst formed in the same event, mud ripples develop in a different flow regime to FIDS, with mud ripples forming under lower density flows, where buoyancy is not significant and shear forces dominate. Consequently, where FIDS ornament mud ripples, it implies that there was subsequent flow transformation to denser flows, as observed elsewhere in decelerating transitional flows (e.g. Baas *et al.*, 2021a, 2021b). These changes in transitional flows are known to alter the degree of turbulence and the length of the recirculation zone in the lee of ripples (Baas & Best, 2008), eventually leading to a cessation of the recirculation zone and formation of a leeside flow expansion region under quasi-laminar plug flows (*sensu* Baas *et al.*, 2009). The transition point between polygonal forms and scales may therefore offer a methodology for determining the dimensions of the recirculation/expansion zone during the formation of FIDS on mud ripples, and thus a methodology for estimating the broad nature of the transitional flow. However, further work is required to examine whether the dynamics of flow over mud ripples exhibit similar characteristics to those examined for the ripples studied by Baas & Best (2008).

High-concentration flow head

The densest part of a subaqueous sediment gravity flow has been shown in many cases to be the head of the flow, or in a smaller flow cell at the very front of the head (Azpiroz-Zabala *et al.*, 2017; Baas *et al.*, 2021a; Pope *et al.*, 2022; McGowan *et al.*, 2024), related to shear stresses and thus erosion being highest at the flow front (Necker *et al.*, 2002; Sequeiros *et al.*, 2009, 2018; Baas *et al.*, 2021a). This flow head, or flow cell, has been shown to be orders of magnitude denser than the rest of the flow (Azpiroz-Zabala *et al.*, 2017; Pope *et al.*, 2022). Outcrops provide evidence for flow heads that are cohesive debris flows (equivalent to quasi-laminar plug flows, *sensu* Baas *et al.*, 2009) capable of forming grooves (Peakall *et al.*, 2020; Baas *et al.*, 2021a), whilst studies of modern examples have argued for high-concentration cohesionless modified grain flows (Pope *et al.*, 2022) or high-concentration weakly turbulent fronts (Talling *et al.*, 2022). Once the head of the flow has moved from an erosional phase to a bypass phase (neither eroding nor depositing, i.e. the equilibrium flows of Crisóstomo-Figueroa *et al.*, 2021), this zone of exceptional high-density, relative to the lower density substrate, could provide the buoyancy force to initiate FIDS. The presence of grooves (Dżułyński & Walton, 1965) or skim marks (Fig. 14), that have been linked to clasts near the front of the flow head (Peakall *et al.*, 2020; Baas *et al.*, 2021a), that cross-cut FIDS, reinforces this concept. The temporal relationships between tool marks and FIDS provide additional insight into the structure of the head or flow cell. In some cases, tool marks and FIDS are formed contemporaneously, with Fig. 2C showing that FIDS can form under conditions suitable for prod marks, which have been linked to flows in the upper transitional plug flow regime (Peakall *et al.*, 2020). Where FIDS are cut by grooves (e.g. Pszonka *et al.*, 2023, fig. 4B) or chevrons (Fig. 10), this suggests that the front of the head is associated with formation of FIDS, and that the tools responsible for groove and

chevron formation that are linked to debris flows (quasi-laminar plug flows; Peakall *et al.*, 2020), are some distance further back from the nose of the current. Collectively, the relationships between FIDS and tool marks suggest that towards the very front of their formative flows, the fluid dynamics are characterized by transitional plug flows, or potentially quasi-laminar plug flows (debris flows), which lack tools interacting with the bed.

As a flow, characterized by a bypass phase, with a debritic, or other high-concentration, head decelerates, it is likely that the more turbiditic component overtakes the head to produce a forerunning turbidity current (Amy *et al.*, 2005; Baas *et al.*, 2021a). In such cases, the more fluidal flow could shape the bed through shear, producing mud ripples in weak cohesive substrates, prior to the arrival of the slower moving head of the denser debritic or high-concentration component (Baas *et al.*, 2021a), which would cause FIDS to develop on the mud ripples.

Implications for palaeosubstrate rheology

The FIDS thus provide substrate information (see Model5 for a range of FIDS on successive beds), demonstrating that the substrate is weak enough to undergo buoyancy-driven diapirism. Furthermore, FIDS can form on top of mud ripples indicating that these mud ripples also reflect relatively weak substrates. In contrast, flutes require a substrate that is sufficiently strong that it can maintain the relatively steep slopes at their upstream 'noses' (Peakall *et al.*, 2020), explaining why flutes and FIDS, and likewise flutes and mud ripples with FIDS, are not found together. An apparent exception to this rule is the occurrence of large flutes on mud ripples with FIDS observed by Winterer (1964), but these were cut at a time when sufficient consolidation had occurred that the steeper sides of the flutes could be maintained, and thus represent a later flow event. In the absence of experiments with extensive measurements of shear strength, it is not possible to quantify the range of substrate strengths that are represented by FIDS, mud ripples and flutes. Nonetheless, they provide a qualitative guide to substrate conditions. Experiments have demonstrated that once beds become strongly consolidated (*ca* 5 to 10 kPa in Yin *et al.*, 2016; equivalent to hard mud in the van Rijn, 1993, scheme), erosion produces flute-like morphologies and potholes, that are analogous to bedrock-river features rather than flutes as observed in deep-marine conditions, thus placing some constraints on an upper limit for flutes (Yin *et al.*, 2016). Allen (1971a) produced flutes with smooth surfaces in pipes using abrasion of modelling clay over periods of 27 to 74 min, although these experiments lacked substrate shear-strength measurements. In contrast, experiments with clearwater flows over 'weakly cohesive' muds (see *Longitudinal ridges and furrows – mechanism 1*) also formed flutes (Allen, 1969). However, these were not smooth as observed in outcrop examples, but instead were covered in smaller structures (such as those in Fig. 12), interpreted as the product of individual eddies. Furthermore, run times were of the order of 3 to 4 min (based on erosion rates, Allen, 1969, table 1). Consequently, it is unclear whether the flutes documented by Allen (1969) were stable, or representative of outcrop examples. Experiments using substrates comprising different strength kaolinite mixtures have demonstrated that various types of chevron marks and striated grooves form in specific substrate conditions, ranging from fluid-solids (>60 Pa) to stiff muds (>160 Pa) (McGowan *et al.*, 2024). Utilizing the approach of McGowan *et al.* (2024) and the example of interrupted chevron marks cutting and deforming wrinkle marks (Fig. 10), provides an estimate of substrate rheology for FIDS, of *ca* 70 to 80 Pa. Thus, collectively, these results suggest that sole structures provide considerable information on substrate rheology. Such substrate information provides an estimate of consolidation times of mud at that interface, and thus a minimum estimate of the time between sediment gravity flow event beds through assuming relationships, such as those in van Rijn (1993). Hence, in systems where sole structures are abundant and mud beds are thin (i.e. the interface is a good guide to the properties of the whole mud bed), their relationships to substrate strength provide the potential for ultra-high-resolution studies (months to centennial scales) of the temporal variability of sediment gravity flows, for rocks that may be hundreds of millions of years old.

Implications for palaeocurrents

Flow-induced interfacial deformation structures (FIDS) are a highly under-used set of sedimentary structures for deriving palaeocurrent measurements, despite their utility being known since the 1960s. FIDS can provide both a sense-of-direction flow indicator (i.e. a bidirectional

indicator), and in the case of some longitudinal ridges and furrows, and scales, an indicator of absolute flow direction. Larger-scale, areally extensive, patterns of ridges and furrows (e.g. Allen, 1982, fig. 1.25, based on Kruit *et al.*, 1975) also provide more detailed information on local palaeocurrents and flow patterns, albeit this is a resource with no real analysis undertaken to date. The recognition that FIDS are related to higher-density flows also suggests that their palaeocurrent directions may differ from lower-density flows that generate scour structures, particularly where flows interact with topography. Such changes have previously been observed between higher-density flows associated with grooves, and lower-density flows related to flutes (Muzzi Magalhaes & Tinterri, 2010; Tinterri & Muzzi Magalhaes, 2011; Bell *et al.*, 2018; Peakall *et al.*, 2020). Consequently, this reinforces the contention of Peakall *et al.* (2020) that palaeocurrents should be differentiated by the type of sedimentary structure as demonstrated by Tinterri *et al.* (2016, 2022), rather than simply analysed as a collective. It is recommended herein that palaeocurrents are analysed separately for the three main categories of sole structures; scour marks, tool marks and FIDS. Furthermore, care needs to be taken to correctly separate FIDS scales from flutes because these are the products of radically different formative flows; scales stack one upon another longitudinally (for example, Fig. 7A), whereas flutes do not, and scales show thin mud layers between their cuspate forms, and do not exhibit the characteristic three-dimensional morphology of flutes (Allen, 1971a).

Depositional environments of FIDS

As a consequence of the limited recognition of FIDS, there are few systematic records of their presence in sedimentary successions. An exception is the study of Dirnerová & Janočko (2014), which showed that longitudinal ridges and furrows are most common in depositional environments that were interpreted as interlobe and channel interdistributary areas. More generally, the present work indicates that FIDS will be found in settings where mud can accumulate, and currents occur that are associated with high-density, cohesive, debritic heads. Consequently, proximal settings such as channels, channel mouth settings and proximal lobes are expected to have few FIDS as a result of the low preservation potential of muds and the erosive nature of the sandstone bases (e.g. Prélat *et al.*, 2009; Brooks *et al.*, 2018; Hubbard *et al.*, 2020; Hodgson *et al.*, 2022; Nieminski *et al.*, 2024). Elevated areas such as external levées and terraces will accumulate muds, but will have few high-density mud-rich flows (e.g. Kane & Hodgson, 2011; Hansen *et al.*, 2015; Baas *et al.*, 2021a). Distal areas, such as the fringes of distal lobe complexes and basin plain deposits, are therefore the most likely palaeoenvironments to generate FIDS, because these have high mud accumulation, transitional mud-rich flows and flat-bedded, non-erosive sands (e.g. Pickering & Hiscott, 1985; Talling *et al.*, 2004; Amy & Talling, 2006; Prélat *et al.*, 2009; Spychala *et al.*, 2017; Baker & Baas, 2020; Tinterri *et al.*, 2022). Whilst these *a priori* arguments can be made, there is a need to test these ideas through detailed field observations across a range of environments.

Differentiating FIDS from load casts and flames

Morphology and processes

Load casts form in reversed density systems and are typically symmetrical in cross-section (Owen, 2003). However, in some cases, the axes of loads and flames can be inclined (Dasgupta, 1998; Moretti *et al.*, 2001; Owen, 2003). The planform orientation of this inclination is generally unclear, as sections are typically two-dimensional and both longitudinal-inclined and transverse-inclined loading has been observed (Moretti *et al.*, 2001). Where observed in planform (Fig. 20), load casts are typically bulbous, equant or elongate (length up to two to four times width; Pettijohn & Potter, 1964; Grumbt, 1966; Potter & Pettijohn, 1977; Allen, 1982, 1985b), in keeping with experimental patterns (Anketell *et al.*, 1970; Allen, 1985b). A planform example is shown in Moretti *et al.* (2001), with a series of elongate ellipsoidal load casts (long axis *ca* 1.3 times greater than the short axis) that are parallel to slope. These load casts, however, lack the planform regularity of FIDS and are quite sparse rather than covering the entire bedding surface, as typically observed in FIDS (see Moretti *et al.*, 2001, plate 46). Transverse elongate load casts are also recognized, developing into elongate pillows if liquefaction is sufficiently long-lasting (Allen, 1982). Inclination of load casts has been linked to: (i) fluid flow (Kuenen & Prentice, 1957; Sanders, 1960; Anketell & Dżułyński, 1968; Postma *et al.*, 2009; Butler *et al.*,

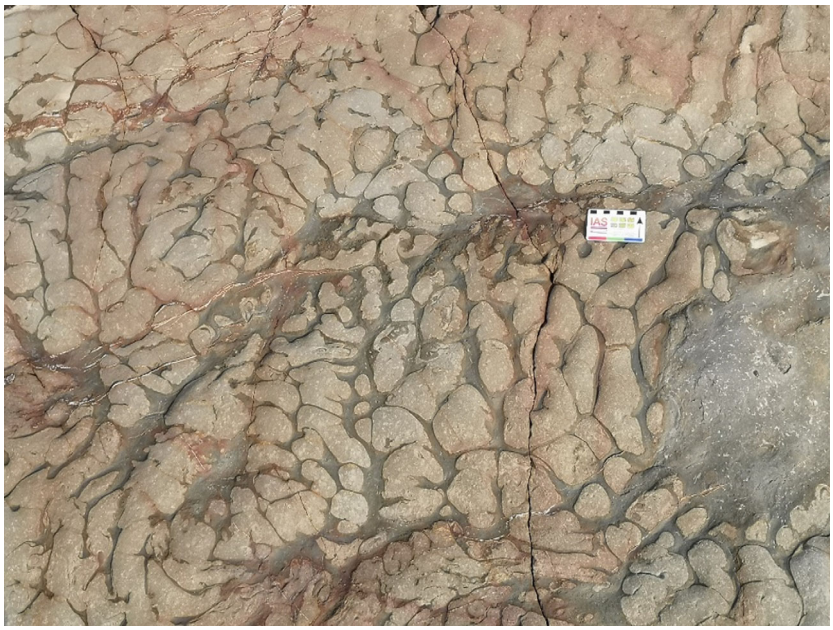

Fig. 20. Load casts seen in planform on the basal surface of a bed. The load casts are broadly equant across the whole surface, and also show appreciable areas of mud-rich sediment (flames). Carboniferous Bude Formation, North Devon, UK. Scale bar shows 1 cm increments. See also Model6.

2016; Tinterri *et al.*, 2016); (ii) fluid flow and sedimentation in turbidity currents that penetrate into a mud bed (Baas *et al.*, 2014, 2016b); (iii) unequal thickness of the overlying sand as a result of erosion, leading to lateral variations in loading (Dasgupta, 1998); and (iv) the downslope component of weight (Moretti *et al.*, 2001; Allen, 2003). Moretti *et al.* (2001) demonstrated in a field example that the structures aligned with the slope, whilst the associated flute and tool marks were oblique to the load cast orientation, indicating that flow drag was not the cause. Experiments also illustrate the importance of the downslope component of weight in generating flames tilted downslope (Moretti *et al.*, 2001). Fluid flow as postulated by Kuenen & Prentice (1957) and Sanders (1960) was inferred but formative mechanisms were not proposed. In contrast, Tinterri *et al.* (2016) argued, based on field data, that an increasing rapidity of deceleration of sediment gravity flows due to interaction with topography leads to increasing inclination of load cast morphology. Furthermore, Anketell & Dżułyński (1968) showed experimentally that, in the case of thin plaster-of-Paris layers over a clay bed, a subsequent dense plaster-of-Paris flow led to two-dimensional load casts, transverse to the flow and tilted downstream. Additional flow related mechanisms, such as flow induced liquefaction (Postma *et al.*, 2009) or shear from kinematic boundary layers (Butler *et al.*, 2016), may also lead to inclined load casts. These mechanisms all differ from those envisaged herein for FIDS and result in load casts that do not form more elongate structures such as those observed in longitudinal ridges and furrows, or scale-like features. A possible exception, however, are the elongate, three-dimensional structures observed by Ninard *et al.* (2022; fig. 6) that bear a striking similarity to longitudinal ridges and furrows. These structures formed between two fluvial sands separated by a thin (tens of millimetres thick) clay layer, with deformation of the overlying cross-beds indicating that they formed post-depositionally rather than during a flow (Ninard *et al.*, 2022, fig. 6A). The structures have been interpreted to be orthogonal to the migration direction of a seismically-induced liquefaction front (Ninard *et al.*, 2022; cf. Anketell *et al.*, 1970, fig. 7). However, scale-like structures (Ninard *et al.*, 2022, fig. 7A) may suggest that the movement of the liquefaction front was parallel to the structures, as in longitudinal ridges and furrows.

Internal structure within load casts and FIDS

Lamination in load casts typically parallels the boundaries of the deformation (e.g. Dżułyński & Walton, 1965; Owen, 2003; Wizevich *et al.*, 2016; Ninard *et al.*, 2022) reflecting the bending of

laminae, or in some cases flow-generated shearing during deformation (Wizevich *et al.*, 2016). In the elongate load casts of Moretti *et al.* (2001), internal layers are inclined in the downstream direction. These laminae relationships differ from those proposed herein for FIDS, where the small vertical length scales of the structures mean that the additional thickness of sand in the furrows relative to the ridges will likely result in very limited additional loading. Thus, any parallel lamination present within the furrows, would not be expected to be significantly deformed from the horizontal (for example, Figs 14B and 15).

Recognition criteria – FIDS versus load casts and flames

Load casts and flames are symmetrical or slightly asymmetrical in cross-section (ellipsoidal in planform), and do not form elongate structures (longer than *ca* two to four times their width), apart from in exceptional circumstances (e.g. Ninard *et al.*, 2022). Furthermore, load casts and flames exhibit laminae that are deformed — typically parallel to the deformation. In contrast, FIDS form far more elongate and regular structures, such as longitudinal ridges and furrows and arcuate scale-like features, or exhibit progressive transitions between structures as a function of morphology, as seen across mud ripples. Furthermore, internal laminae are not concordant with deformation. A further difference is that FIDS are always thin (millimetres to tens of millimetres), whilst load casts can be metres in depth in some cases (e.g. Van der Merwe *et al.*, 2009; Taşgin *et al.*, 2011; Gruszka *et al.*, 2016; Wizevich *et al.*, 2016). This reflects the weak but coherent substrates required for FIDS, whilst large load casts can form via large-scale liquefaction of the underlying bed (Allen, 1982).

Challenges to the understanding of FIDS

Linking the existing literature on sole marks that are herein classified as FIDS, largely from the 1960s and early 1970s, to the subsequent advances in understanding of sediment gravity flows, and the fluid dynamics of systems with varying buoyancy and shear, has enabled a new model for FIDS to be proposed. However, there remain challenges to understanding these structures. A key missing component is information on the nature of the overlying beds; what are the relationships between bed types and FIDS? This lack of data is even greater than that observed for flutes and grooves, where some work had examined the relationship between sole mark type and Bouma divisions (Bouma, 1962; Pett & Walker, 1971; Crimes, 1973; see table 1 of Peakall *et al.*, 2020), although this early work was limited by a lack of recognition of more recently identified bed types such as hybrid event beds (Haughton *et al.*, 2003, 2009) and transitional flow deposits (*sensu* Privat *et al.*, 2024; see also Baker & Baas, 2020; Taylor *et al.*, 2024). More recent studies have begun to address the nature of flutes and tool marks and their overlying beds utilizing a modern approach to bed types (Baas *et al.*, 2021a). A similar approach for FIDS would be beneficial. Similarly, there is no information on the nature of the mud beds, their thickness, and whether there is any broader zone of deformation associated with them. In turn, these bed relationships need to be integrated with a broader understanding of where FIDS are found in terms of sub-environments.

There is also a need to improve the understanding of the formation of FIDS. In particular, the three-dimensional nature of scales is poorly known, and would benefit from studies examining serial cut and polished sections through these features, or possibly detailed computerized tomography (CT) scanning, tied to thin-section analysis to identify the distribution of laminae. Such analysis would address limitations in present understanding, such as the presence of scales that are more closely spaced longitudinally, than the width of their furrows. Physical experimentation, with measurement of flow and substrate properties, would also enable an improved understanding of the substrate rheology required for FIDS development (cf. McGowan *et al.*, 2024). As highlighted in Peakall *et al.* (2020), there has been abundant research on aggradational bedforms such as ripples and dunes in the past half-century (e.g. Baas *et al.*, 2016a, 2019; Vinent *et al.*, 2019), but remarkably little work on sole structures. The recognition that FIDS, and sole marks in general, contain information on flow characteristics, flow transformation, the longitudinal distribution of flows and substrate rheology, in addition to palaeocurrent indicators, makes the case for further research to tackle the challenges highlighted herein.

CONCLUSIONS

Herein, it is argued that weak, cohesive substrates may actively deform as flows travel across them,

and that the action of the overriding flow (shear), and the density difference (buoyancy) between the less dense substrate and the denser overlying flow, determine the type of sedimentary structures formed. Analogies are drawn between these sedimentary structures and pattern analysis obtained from classical fluid dynamics experiments examining the interaction of buoyancy versus shear forces. This group of sole marks is herein termed flow-induced interfacial deformation structures (FIDS), and includes longitudinal ridges and furrows, scales (cuspate marks that open downflow), polygonal structures, and collectively the 'dinosaur leather' that covers many mud ripples. Transverse wrinkles may be formed by strong shear and weak buoyancy, or by pure shear. This new process model challenges long held concepts: longitudinal ridges and furrows have been predominantly considered to be scour marks for the past 60 years, and structures on mud ripples have been linked to individual eddies within a turbulent flow for over 50 years. FIDS represent a third group of sole marks alongside scour marks and tool marks. They are highly under-utilized as palaeocurrent indicators, with the direction of the scales being known as a unidirectional indicator since the 1960s, but little used today. It is also demonstrated that FIDS provide information beyond just palaeocurrents, indicating the passage of dense flows above weak muddy substrates, which means that they likely develop, and preserve, preferentially in relatively distal depositional environments. The ornamentation of FIDS across mud ripples points to a temporal flow transformation with flows becoming denser with time. This new knowledge of the formative mechanisms, and utility, of flow-induced interfacial deformation structures, can be integrated with recent work on the mechanics and uses of scour marks and tool marks, to make sole marks an important source of sedimentological information, moving beyond purely palaeocurrent analysis.

ACKNOWLEDGEMENTS

JP, JB and JHB are grateful to the UK Natural Environment Research Council for grant NE/C514823/1 that enabled our initial work on transitional flows. JP, JB, JHB and PŁ thank Alfred Uchman, Tomasz Pyrcz, Bartłomiej Kajdas and Robert Czuchnowski for access to the Natural Sciences Education Centre at the Jagiellonian University, and for showing us sole marks in and around the Carpathians. Funding from the Jack and Richard C. Threet chair in Sedimentary Geology supported some of the work reported herein. Priya Subramanian is thanked for providing and modifying Fig. 18, and for associated discussion; Dan Matsumoto and Hajime Naruse are thanked for supplying an original of Fig. 9. Gareth Keevil is thanked for help with Figs 4 and 8. We thank reviewers Peter Haughton, Marco Patacci and Roberto Tinterri for their extremely insightful comments, and editors Fabrizio Felletti and Piret Plink-Björklund.

DATA AVAILABILITY STATEMENT

This is a State of the Science paper, and does not contain any primary data.

REFERENCES

Allen, J.R.L. (1966) Note on the use of plaster of Paris in flow visualization, and some geological applications. *J. Fluid Mech.*, **25**, 331–335.

Allen, J.R.L. (1969) Erosional current marks of weakly cohesive beds. *J. Sed. Petrol.*, **39**, 607–623.

Allen, J.R.L. (1971a) Transverse erosional marks of mud and rock: their physical basis and geological significance. *Sed. Geol.*, **5**, 167–385.

Allen, J.R.L. (1971b) Mixing at turbidity current heads, and its geological implications. *J. Sed. Petrol.*, **50**, 227–234.

Allen, J.R.L. (1982) *Sedimentary Structures: Their Character and Physical Basis, Volume II*, p. 663. Elsevier, Amsterdam.

Allen, J.R.L. (1985a) Wrinkle marks: an intertidal sedimentary structure due to aseismic soft-sediment loading. *Sed. Geol.*, **41**, 75–95.

Allen, J.R.L. (1985b) *Principles of Physical Sedimentology*, p. 272. Allen and Unwin, London.

Allen, J.R.L. (2003) Load structures. In: *Encyclopedia of Sediments and Sedimentary Rocks* (Eds Middleton, G.V., Church, M.J., Coniglio, M., Hardie, L.A. and Langstaffe, F.J.), pp. 413–414. Kluwer Academic Publishers, Dordrecht.

Amy, L. and **Talling, P.J.** (2006) Anatomy of turbidites and linked debrites based on long distance (120 × 30 km) bed correlation, Marnoso Arenacea Formation, Northern Apennines, Italy. *Sedimentology*, **53**, 161–212.

Amy, L.A., **Peakall, J.** and **Talling, P.J.** (2005) Density- and viscosity-stratified gravity currents: insights from laboratory experiments and implications for flow deposits. *Sed. Geol.*, **179**, 5–29.

Anketell, J.M. and **Dżułyński, S.** (1968) Transverse deformational patterns in unstable sediments. *Ann. Soc. Géol. Pologne*, **38**, 411–416.

Anketell, J.M., **Cegla, J.** and **Dżułyński, S.** (1970) On the deformational structures in systems with reversed density gradients. *Ann. Soc. Géol. Pologne*, **40**, 3–30.

Azpiroz-Zabala, M., **Cartigny, M.J.B.**, **Talling, P.J.**, **Parsons, D.R.**, **Sumner, E.J.**, **Clare, M.A.**, **Simmons, S.M.**, **Cooper, C.** and **Pope, E.L.** (2017) Newly recognized turbidity

current structure can explain prolonged flushing of submarine canyons. *Sci. Adv.*, **3**, e1700200.

Baas, J.H. and **Best, J.L.** (2002) Turbulence modulation in clay-rich sediment-laden flows and some implications for sediment deposition. *J. Sed. Res.*, **72**, 336–340.

Baas, J.H. and **Best, J.L.** (2008) The dynamics of turbulent, transitional and laminar clay-laden flow over a fixed current ripple. *Sedimentology*, **55**, 635–666.

Baas, J.H., **Best, J.L.**, **Peakall, J.** and **Wang, M.** (2009) A phase diagram for turbulent, transitional, and laminar clay suspension flows. *J. Sed. Res.*, **79**, 162–183.

Baas, J.H., **Best, J.L.** and **Peakall, J.** (2011) Depositional processes, bedform development and hybrid flows in rapidly decelerated cohesive (mud–sand) sediment flows. *Sedimentology*, **58**, 1953–1987.

Baas, J.H., **Manica, R.**, **Puhl, E.**, **Verhagen, I.** and **Borges, A.L.O.** (2014) Processes and products of turbidity currents entering soft muddy substrates. *Geology*, **42**, 371–374.

Baas, J.H., **Best, J.L.** and **Peakall, J.** (2016a) Predicting bedforms and primary current stratification in cohesive mixtures of mud and sand. *J. Geol. Soc. Lond.*, **173**, 12–45.

Baas, J.H., **Manica, R.**, **Puhl, E.** and **Borges, A.L.O.** (2016b) Thresholds of intrabed flow and other interactions of turbidity currents with soft muddy substrates. *Sedimentology*, **63**, 2002–2036.

Baas, J.H., **Baker, M.L.**, **Malarkey, J.**, **Bass, S.J.**, **Manning, A.J.**, **Hope, J.A.**, **Peakall, J.**, **Lichtman, I.D.**, **Ye, L.**, **Davies, A.G.**, **Parsons, D.R.**, **Paterson, D.M.** and **Thorne, P.D.** (2019) Integrating field and laboratory approaches for ripple development in mixed sand-clay-EPS. *Sedimentology*, **66**, 2749–2768.

Baas, J.H., **Tracey, N.D.** and **Peakall, J.** (2021a) Sole marks reveal deep-marine depositional process and environment: implications for flow transformation and hybrid event bed models. *J. Sed. Res.*, **91**, 986–1009.

Baas, J.H., **Best, J.L.** and **Peakall, J.** (2021b) Rapid gravity flow transformation revealed in a single climbing ripple. *Geology*, **49**, 493–497.

Baas, J.H., **Baker, M.L.**, **Buffon, P.**, **Strachan, L.J.**, **Bostock, H.C.**, **Hodgson, D.**, **Eggenhuisen, J.T.** and **Spychala, Y.T.** (2022) Blood, lead and spheres: a hindered settling equation for sedimentologists based on metadata analysis. *Depos. Rec.*, **8**, 603–615.

Bagnold, R.A. (1954) Experiments on a gravity-free dispersion of large solid spheres in a Newtonian fluid under shear. *Proc. R. Soc. Lond.*, **225**, 49–63.

Baker, M.L. and **Baas, J.H.** (2020) Mixed sand–mud bedforms produced by transient turbulent flows in the fringe of submarine fans: indicators of flow transformation. *Sedimentology*, **67**, 2645–2671.

Baker, M.L., **Baas, J.H.**, **Malarkey, J.**, **Silva Jacinto, R.**, **Craig, M.J.**, **Kane, I.A.** and **Barker, S.** (2017) The effect of clay type on the properties of cohesive sediment gravity flows and their deposits. *J. Sed. Res.*, **87**, 1176–1195.

Basilici, G., **de Luca, P.H.V.** and **Poire, D.G.** (2012) Hummocky cross-stratification-like structures and combined-flow ripples in the Punta Negra Formation (Lower-Middle Devonian, Argentine Precordillera): a turbiditic deep-water or storm-dominated prodelta inner-shelf system? *Sed. Geol.*, **267–268**, 73–92.

Bell, D., **Stevenson, C.J.**, **Kane, I.A.**, **Hodgson, D.M.** and **Poyatos-Moré, M.** (2018) Topographic controls on the development of contemporaneous but contrasting basin-floor depositional architectures. *J. Sed. Res.*, **88**, 1166–1189.

Best, J. (1992) On the entrainment of sediment and initiation of bed defects: insights from recent developments within turbulent boundary layer research. *Sedimentology*, **39**, 797–811.

Best, J.L. and **Leeder, M.R.** (1993) Drag reduction in turbulent muddy seawater flows and some sedimentary consequences. *Sedimentology*, **40**, 1129–1137.

Blanchard, S., **Matheson, E.J.**, **Fielding, C.R.**, **Best, J.L.**, **Bryk, A.B.**, **Howell, K.J.**, **Monson, C.C.**, **Mahoney, G.** and **Peakall, J.** (2019) Early burial mud diapirism and its impact on stratigraphic architecture in the Carboniferous of the Shannon Basin, County Clare, Ireland. *Sedimentology*, **66**, 329–361.

Bodenschatz, E., **Pesch, W.** and **Ahlers, G.** (2000) Recent developments in Rayleigh-Bénard convection. *Annu. Rev. Fluid Mech.*, **32**, 709–778.

Boggs, S., Jr. (2014) *Principles of Sedimentology and Stratigraphy*, 5th edn, p. 564. Pearson, Harlow.

Bouma, A. (1962) *Sedimentology of Some Flysch Deposits: A Graphic Approach to Facies Interpretation*, p. 168. Elsevier, Amsterdam/New York.

Bridge, J.S. and **Demicco, R.V.** (2008) *Earth Surface Processes, Landforms and Sediment Deposits*, p. 815. Cambridge University Press, Cambridge.

Brooks, H.B., **Hodgson, D.M.**, **Brunt, R.L.**, **Peakall, J.**, **Hofstra, M.** and **Flint, S.S.** (2018) Deepwater channel-lobe transition zone dynamics: processes and depositional architecture, an example from the Karoo Basin, South Africa. *Geol. Soc. Am. Bull.*, **130**, 1723–1746.

Butler, R.W.H., **Eggenhuisen, J.T.**, **Haughton, P.** and **McCaffrey, W.D.** (2016) Interpreting syndepositional sediment remobilization and deformation beneath submarine gravity flows; a kinematic boundary layer approach. *J. Geol. Soc. Lond.*, **173**, 46–58.

Cantero, M.I., **Cantelli, A.**, **Pirmez, C.**, **Balchander, S.**, **Mohrig, D.**, **Hickson, T.A.**, **Yeh, T.H.**, **Naruse, H.** and **Parker, G.** (2012) Emplacement of massive turbidites linked to extinction of turbulence in turbidity currents. *Nat. Geosci.*, **5**, 42–45.

Cantero, M.I., **Balachander, S.**, **Cantelli, A.** and **Parker, G.** (2014) A simplified approach to address turbulence modulation in turbidity currents as a response to slope breaks and loss of lateral confinement. *Environ. Fluid Mech.*, **14**, 371–385.

Chadwick, G.H. (1948) Ordovician "dinosaur-leather" markings (Abstract). *Geol. Soc. Am. Bull.*, **59**, 1315.

Collinson, J. and **Mountney, N.** (2019) *Sedimentary Structures*, 4th edn, p. 340. Dunedin Academic Press, Edinburgh, UK.

Craig, G.Y. and **Walton, E.K.** (1962) Sedimentary structures and palaeocurrent directions from the Silurian rocks of Kirkcudbrightshire. *Trans. Edinb. Geol. Soc.*, **19**, 100–119.

Crimes, T.P. (1973) From limestones to distal turbidites: a facies and trace fossil analysis in the Zumaya flysch (Paleocene-Eocene), North Spain. *Sedimentology*, **20**, 105–131.

Crisóstomo-Figueroa, A., **McArthur, A.D.**, **Dorrell, R.M.**, **Amy, L.** and **McCaffrey, W.D.** (2021) A new modelling approach to sediment bypass prediction applied to the East Coast Basin, New Zealand. *Geol. Soc. Am. Bull.*, **133**, 1734–1748.

Dai, A. and **Huang, Y.-L.** (2022) On the merging and splitting processes in the lobe-and-cleft structure at a gravity head. *J. Fluid Mech.*, **930**, A6.

Daly, B. (1968) Sedimentary structures from a non-marine horizon in the Bembridge Marls (Oligocene) of the Isle of Wight, Hampshire, England. *J. Sed. Petrol.*, **38**, 114–127.

Daniels, K.E., **Plapp, B.B.** and **Bodenschatz, E.** (2000) Pattern formation in inclined layer convection. *Phys. Rev. Lett.*, **84**, 5320–5323.

Dasgupta, P. (1998) Recumbent flame structures in the Lower Gondwana rocks of the Jharia Basin, India – a plausible origin. *Sed. Geol.*, **119**, 253–261.

Davies, N.S. and **Shillito, A.P.** (2021) True substrates: the exceptional resolution and unexceptional preservation of deep time snapshots on bedding surfaces. *Sedimentology*, **68**, 3307–3356.

Davies, N.S., **Liu, A.G.**, **Gibling, M.R.** and **Miller, R.F.** (2016) Resolving MISS conceptions and misconceptions: a geological approach to sedimentary surface textures generated by microbial and abiotic processes. *Earth-Sci. Rev.*, **154**, 210–246.

Diplas, P., **Dancey, C.L.**, **Celik, A.O.**, **Valyrakis, M.**, **Greer, K.** and **Akar, T.** (2008) The role of impulse on the initiation of particle movement under turbulent flow conditions. *Science*, **322**, 717–720.

Dirnerová, D. and **Janočko, J.** (2014) Sole structures as a tool for depositional environment interpretation; a case study from the Oligocene Cergowa Sandstone, Dukla Unit (Outer Carpathians, Slovakia). *Geol. Q.*, **58**, 41–50.

Dżułyński, S. (1965) New data on experimental production of sedimentary structures. *J. Sed. Petrol.*, **35**, 196–212.

Dżułyński, S. (1966) Sedimentary structures resulting from convection-like pattern of motion. *Ann. Soc. Géol. Pologne*, **36**, 3–21.

Dżułyński, S. (1996) Erosional and deformational structures in single sedimentary beds: a genetic commentary. *Ann. Soc. Geol. Pol.*, **66**, 101–189.

Dżułyński, S. (2001) *Atlas of Sedimentary Structures from the Polish Flysch Carpathians*. 12th meeting of the Association of European Geological Societies, 132 pp.

Dżułyński, S. and **Sanders, J.E.** (1962) Current marks on firm mud bottoms. *Trans. Connecticut Acad. Arts Sci.*, **42**, 57–96.

Dżułyński, S. and **Simpson, F.** (1966a) Experiments on interfacial current markings. *Geol. Romana*, **5**, 197–214.

Dżułyński, S. and **Simpson, F.** (1966b) Influence of bottom irregularities and transported tools upon experimental scour markings. *Ann. Soc. Géol. Pologne*, **36**, 285–294.

Dżułyński, S. and **Walton, E.K.** (1963) Experimental production of sole markings. *Trans. Edinb. Geol. Soc.*, **19**, 279–305.

Dżułyński, S. and **Walton, E.K.** (1965) *Sedimentary Features of Flysch and Greywackes. Developments in Sedimentology 7*, p. 274. Elsevier, Amsterdam.

Edwards, D.E., **Leeder, M.R.**, **Best, J.L.** and **Pantin, H.M.** (1994) An experimental study of reflected density currents and the interpretation of certain turbidites. *Sedimentology*, **41**, 437–461.

Graham, A. (1933) Shear pattern in an unstable layer of air. *Phil. Trans. R. Soc. London*, **232**, 285–296.

Grumbt, E. (1966) Schichtungstypen, marken und synsedimentäre deformationsgefüge im Buntsandstein Südthüringens. *Ber. dtsch. Ges. Geol. Wiss. Reihe A Geol. Paläontol.*, **11**, 217–234.

Gruszka, B., **Ford, A.M.** and **van Loon, A.J.** (2016) A fluctuating ice front over an esker near Ryssjön (S Sweden) as a cause of a giant load cast. *Sed. Geol.*, **344**, 47–56.

Hansen, L.A.S., **Callow, R.H.T.**, **Kane, I.A.**, **Gamberi, F.**, **Rovere, M.**, **Cronin, B.T.** and **Kneller, B.C.** (2015) Genesis and character of thin-bedded turbidites associated with submarine channels. *Mar. Petrol. Geol.*, **67**, 852–879.

Harrison, P. and **Maltman, A.** (2003) Numerical modelling of reverse-density structures in soft non-Newtonian sediments. In: *Subsurface Sediment Mobilization* (Eds Van Rensbergen, P., Hillis, R.R., Maltman, A.J. and Morley, C.K.), *Geological Society of London Special Publication*, **216**, 35–50.

Haughton, P.D., **Barker, S.P.** and **McCaffrey, W.D.** (2003) 'Linked' debrites in sand-rich turbidite systems–origin and significance. *Sedimentology*, **50**, 459–482.

Haughton, P., **Davis, C.**, **McCaffrey, W.** and **Barker, S.** (2009) Hybrid sediment gravity flow deposits classification, origin and significance. *Mar. Petrol. Geol.*, **26**, 1900–1918.

Heifetz, E., **Agnon, A.** and **Marco, S.** (2005) Soft sediment deformation by Kelvin Helmholtz instability: a case study from Dead Sea earthquakes. *Earth Planet. Sci. Lett.*, **236**, 497–504.

Hill, J., **Rush, G.**, **Peakall, J.**, **Johnson, M.**, **Hodson, L.**, **Barlow, N.L.M.**, **Bowman, E.T.**, **Gehrels, W.R.**, **Hodgson, D.M.** and **Kesserwani, G.** (2023) Resolving tsunami wave dynamics: integrating sedimentology and numerical modelling. *Depos. Rec.*, **9**, 1046–1065.

Hiscott, R.N. (1994) Traction-carpet stratification in turbidites – fact or fiction. *J. Sed. Res.*, **64**, 204–208.

Hodgson, D.M., **Peakall, J.** and **Maier, K.L.** (2022) Submarine channel mouth settings: processes, geomorphology, and deposits. *Front. Earth Sci.*, **10**, 790320.

Hubbard, S.M., **Jobe, Z.R.**, **Romans, B.W.**, **Covault, J.A.**, **Sylvester, Z.** and **Fildani, A.** (2020) The stratigraphic evolution of a submarine channel: linking seafloor dynamics to depositional products. *J. Sed. Res.*, **90**, 673–686.

Hudec, M.R. and **Jackson, M.P.A.** (2007) Terra infirma: understanding salt tectonics. *Earth-Sci. Rev.*, **82**, 1–28.

Kane, I.A. and **Hodgson, D.M.** (2011) Sedimentological criteria to differentiate submarine channel–levee subenvironments: exhumed examples from the Rosario Fm. (Upper Cretaceous) of Baja California, Mexico, and the Fort Brown Fm. (Permian), Karoo Basin, S. Africa. *Mar. Petrol. Geol.*, **28**, 807–823.

Kelling, G. and **Walton, E.K.** (1957) Load-cast structures: their relationship to upper-surface structures and their mode of formation. *Geol. Mag.*, **94**, 481–491.

Kline, S.J., **Reynolds, W.C.**, **Schraub, F.A.** and **Rundstadler, P.W.** (1967) The structure of turbulent boundary layers. *J. Fluid Mech.*, **30**, 741–773.

Kostaschuk, R., **Nasr-Azadani, M.M.**, **Meiburg, E.**, **Wei, T.**, **Chen, Z.**, **Negretti, M.E.**, **Best, J.**, **Peakall, J.** and **Parsons, D.R.** (2018) On the causes of pulsing in continuous turbidity currents. *J. Geophys. Res. Earth*, **123**, 2827–2843.

Kruit, C., **Brower, J.**, **Knox, G.**, **Schollnberger, W.** and **van Vliet, A.** (1975) *Une excursion aux cones d'alluvions en eau profonde d'age Tertiaire près de San Sebastian (Province de Guipuzcoa, Espagne)*. Excursion 23, IX Congrès International de Sedimentologie, Nice, 1975, 75 pp.

Kuenen, P. (1957) Sole markings of graded greywacke beds. *J. Geol.*, **65**, 231–258.

Kuenen, P. and **Menard, H.W.** (1952) Turbidity currents, graded and non-graded deposits. *J. Sed. Petrol.*, **22**, 83–96.

Kuenen, P. and **Prentice, J.E.** (1957) Flow-markings and lode-casts. *Geol. Mag.*, **94**, 173–174.

Leeder, M. (2011) *Sedimentology and Sedimentary Basins: From Turbulence to Tectonics*, p. 768. Wiley-Blackwell, Oxford.

de Luca, P.H.V. and **Basilici, G.** (2013) A prodeltaic system controlled by hyperpycnal flows and storm waves:

reinterpretation of the Punta Negra Formation (Lower-Middle Devonian, Argentine Precordillera). *Braz. J. Geol.*, **43**, 673–694.

Matsumoto, D., **Naruse, H.**, **Fujino, S.**, **Surphawajruksakul, A.**, **Jarupongsakul, T.**, **Sakakura, N.** and **Murayama, M.** (2008) Truncated flame structures within a deposit of the Indian Ocean Tsunami: evidence of syn-sedimentary deformation. *Sedimentology*, **55**, 1559–1570.

McGowan, D., **Salian, A.**, **Baas, J.H.**, **Peakall, J.** and **Best, J.** (2024) On the origin of chevron marks and striated grooves, and their use in predicting mud bed rheology. *Sedimentology*, **71**, 687–708.

Menzoul, B., **Stow, D.**, **Adaci, M.**, **Benhamou, M.**, **Araibi, H.M.**, **Bensalah, M.** and **Benyoucef, M.** (2019) Deepwater sediment facies and sole marks of the Numidian Flysch, Algeria. In: *Paleobidiversity and Tectono-Sedimentary Records in the Mediterranean Tethys and Related Eastern Areas* (Eds Boughdiri, M., Bádenas, B., Selden, P., Jaillard, E., Bengtson, P. and Granier, B.R.C.), pp. 241–243. Advances in Science, Technology and Innovation. Springer Nature Switzerland AG, Cham.

Moretti, M., **Soria, J.M.**, **Alfaro, P.** and **Walsh, N.** (2001) Asymmetrical soft-sediment deformation structures triggered by rapid sedimentation in turbiditic deposits (Late Miocene, Guadix Basin, Southern Spain). *Facies*, **44**, 283–294.

Muzzi Magalhaes, P. and **Tinterri, R.** (2010) Stratigraphy and depositional setting of slurry and contained (reflected) beds in the Marnoso-arenacea Formation (Langhian-Serravallian) Northern Apennines, Italy. *Sedimentology*, **57**, 1685–1720.

Necker, F., **Härtel, C.**, **Kleiser, L.** and **Meiburg, E.** (2002) High-resolution simulations of particle-driven gravity currents. *Int. J. Multiphase Flow*, **28**, 279–300.

Nichols, G. (2009) *Sedimentology and Stratigraphy*, 2nd edn, p. 419. Wiley-Blackwell, Chichester, UK.

Nieminski, N.M., **McHargue, T.R.**, **Gooley, J.T.**, **Fildani, A.** and **Lowe, D.R.** (2024) Spatial distribution and variability of lobe facies in a large sand-rich submarine fan system: Neoproterozoic Zerrissene Group, Namibia. *Sedimentology*, **71**, 81–115.

Ninard, K., **Łapcik, P.**, **Uchman, A.** and **Stachacz, M.** (2022) 3D sine wave-like geometry of soft sediment deformation structures: possible record of the Late Pleistocene seismic activity over the Teisseyre-Tornquist Zone. *Terra Nova*, **34**, 54–61.

Owen, G. (2003) Load structures: gravity-driven sediment mobilization in the shallow subsurface. In: *Subsurface Sediment Mobilization* (Eds Van Rensbergen, P., Hillis, R.R., Maltman, A.J. and Morley, C.K.), *Geological Society of London Special Publication*, **216**, 21–34.

Parkash, B. and **Middleton, G.V.** (1970) Downcurrent textural changes in Ordovician turbidite graywackes. *Sedimentology*, **14**, 259–293.

Peakall, J., **Best, J.L.**, **Baas, J.**, **Hodgson, D.M.**, **Clare, M.A.**, **Talling, P.J.**, **Dorrell, R.M.** and **Lee, D.R.** (2020) An integrated process-based model of flutes and tool marks in deep-water environments: implications for palaeohydraulics, the Bouma sequence, and hybrid event beds. *Sedimentology*, **67**, 1601–1666.

Pett, J.W. and **Walker, R.G.** (1971) Relationship of flute cast morphology to internal sedimentary structures in turbidites. *J. Sed. Petrol.*, **41**, 114–128.

Pettijohn, F.J. and **Potter, P.W.** (1964) *Atlas and Glossary of Primary Sedimentary Structures*, p. 370. Springer-Verlag, Berlin.

Pickering, K.T. and **Hiscott, R.N.** (1985) Contained (reflected) turbidity currents from the Middle Ordovician Cloridorme Formation, Quebec, Canada: an alternative to the antidune hypothesis. *Sedimentology*, **32**, 373–394.

Pope, E.L., **Cartigny, M.J.B.**, **Clare, M.A.**, **Talling, P.J.**, **Lintern, D.G.**, **Vellinga, A.**, **Hage, S.**, **Açikalin, S.**, **Bailey, L.**, **Chapplow, N.**, **Chen, Y.**, **Eggenhuisen, J.T.**, **Hendry, A.**, **Heerema, C.J.**, **Heijnen, M.S.**, **Hubbard, S.M.**, **Hunt, J.E.**, **McGhee, C.**, **Parsons, D.R.**, **Simmons, S.M.**, **Stacey, C.D.** and **Vendettuoli, D.** (2022) First source-to-sink monitoring shows dense head controls sediment flux and runout in turbidity currents. *Sci. Adv.*, **8**, eabj3220.

Porada, H. and **Bouougri, E.** (2007) 'Wrinkle structures' – a critical review. In: *Atlas of Microbial Mat Features Preserved within the Clastic Rock Record* (Eds Schieber, J., Bose, P.K., Eriksson, P.G., Banerjee, S., Sarkar, S., Altermann, W. and Catuneau, O.), pp. 135–144. Elsevier, Amsterdam.

Postma, G., **Cartigny, M.** and **Kleverlaan, K.** (2009) Structureless, coarse-tail graded Bouma Ta formed by internal hydraulic jump of the turbidity current? *Sed. Geol.*, **219**, 1–6.

Potter, P.E. and **Pettijohn, F.J.** (1977) *Paleocurrents and Basin Analysis*, 2nd edn, p. 425. Academia Press, New York.

Prélat, A., **Hodgson, D.M.** and **Flint, S.S.** (2009) Evolution, architecture and hierarchy of distributary deep-water deposits: a high-resolution outcrop investigation from the Permian Karoo Basin, South Africa. *Sedimentology*, **56**, 2132–2154.

Privat, A.M.-L.J., **Peakall, J.**, **Hodgson, D.M.**, **Schwarz, E.**, **Jackson, C.A.-L.** and **Arnol, J.A.** (2024) Evolving fill-and-spill patterns across linked early post-rift depocentres control lobe characteristics: Los Molles Formation, Argentina. *Sedimentology*, **71**, 1639–1685.

Pszonka, J., **Wendorff, M.** and **Godlewski, P.** (2023) Sensitivity of marginal basins in recording global icehouse and regional tectonic controls on sedimentation. Example of the Cergowa Basin, (Oligocene) Outer Carpathians. *Sed. Geol.*, **444**, 106326.

Reineck, H.-E. (1969) Die entstehung von runzelmarken. *Nat. Mus.*, **99**, 386–388.

Reineck, H.-E. and **Singh, I.B.** (1980) *Depositional Sedimentary Environments*, 2nd edn, p. 549. Springer-Verlag, Berlin.

Ricci Lucchi, F. (1995) *Sedimentographica: A Photographic Atlas of Sedimentary Structures*, 2nd edn, p. 255. Columbia University Press, New York.

van Rijn, L.C. (1993) *Principles of Sediment Transport in Rivers, Estuaries and Coastal Seas*, p. 700. Aqua Publications, Amsterdam.

Sanders, J.E. (1960) Origin of convoluted laminae. *Geol. Mag.*, **97**, 409–421.

Sequeiros, O.E., **Naruse, H.**, **Endo, N.**, **Garcia, M.H.** and **Parker, G.** (2009) Experimental study on self-accelerating turbidity currents. *J. Geophys. Res. Oceans*, **114**, C05025. https://doi.org/10.1029/2008JC005149.

Sequeiros, O.E., **Mosquera, R.** and **Pedocchi, F.** (2018) Internal structure of a self-accelerating turbidity current. *J. Geophys. Res. Oceans*, **123**, 6260–6276.

Simpson, J.E. (1972) Effects of the lower boundary on the head of a gravity current. *J. Fluid Mech.*, **53**, 759–768.

Simpson, J.E. (1997) *Gravity Currents: In the Environment and the Laboratory*, 2nd edn, p. 244. Cambridge University Press, Cambridge.

Spychala, Y.T., **Hodgson, D.M.**, **Prélat, A.**, **Kane, I.A.**, **Flint, S.S.** and **Mountney, N.P.** (2017) Frontal and lateral

submarine lobe fringes: comparing sedimentary facies, architecture and flow processes. *J. Sed. Res.*, **87**, 75–96.

Stow, D.A.V. (2005) *Sedimentary Rocks in the Field*, p. 320. Manson Publishing, London.

Subramanian, P., **Brausch, O.**, **Daniels, K.E.**, **Bodenschatz, E.**, **Schneider, T.M.** and **Pesch, W.** (2016) Spatio-temporal patterns in inclined layer convection. *J. Fluid Mech.*, **794**, 719–745.

Talling, P.J. (2013) Hybrid submarine flows comprising turbidity current and cohesive debris flow: deposits, theoretical and experimental analyses, and generalized models. *Geosphere*, **9**, 460–488.

Talling, P.J., **Amy, L.A.**, **Wynn, R.B.**, **Peakall, J.** and **Robinson, M.** (2004) Beds comprising debrite sandwiched within co-genetic turbidite: origin and widespread occurrence in distal depositional environments. *Sedimentology*, **51**, 163–194.

Talling, P.J., **Baker, M.L.**, **Pope, E.L.**, **Ruffell, S.C.**, **Silva Jacinto, R.**, **Heijnen, M.S.**, **Hage, S.**, **Simmons, S.M.**, **Hasenhündl, M.**, **Heerema, C.J.**, **McGhee, C.**, **Apprioual, R.**, **Ferrant, A.**, **Cartigny, M.J.B.**, **Parsons, D.R.**, **Clare, M.A.**, **Tshimanga, R.M.**, **Trigg, M.A.**, **Cula, C.A.**, **Faria, R.**, **Gaillot, A.**, **Bola, G.**, **Wallance, D.**, **Griffiths, A.**, **Nunny, R.**, **Urlaub, M.**, **Peirce, C.**, **Burnett, R.**, **Neasham, J.** and **Hilton, R.J.** (2022) Longest sediment flows yet measured show how major rivers connect efficiently to deep sea. *Nat. Commun.*, **13**, 4193.

Taşgin, C.K., **Orhan, H.**, **Türkmen, İ.** and **Aksoy, E.** (2011) Soft-sediment deformation structures in the late Miocene Şelmo Formation around Adiyaman area, Southeastern Turkey. *Sed. Geol.*, **235**, 277–291.

Taylor, W.J., **Hodgson, D.M.**, **Peakall, J.**, **Kane, I.A.**, **Morris, E.A.** and **Flint, S.S.** (2024) Unidirectional and combined transitional flow bedforms: controls on process and distribution in submarine slope settings. *Sedimentology*, **71**, 1329–1362.

Tinterri, R. and **Muzzi Magalhaes, P.** (2011) Synsedimentary structural control on foredeep turbidites related to basin segmentation: facies response to the increase in tectonic confinement (Marnoso-arenacea Formation, Miocene, Northern Apennines, Italy). *Mar. Petrol. Geol.*, **67**, 81–110.

Tinterri, R., **Muzzi Magalhaes, P.**, **Tagliaferri, A.** and **Cunha, R.S.** (2016) Convolute laminations and load structures in turbidites as indicators of flow reflections and decelerations against bounding slopes. Examples from the Marnoso-arenacea Formation (northern Italy) and Annot Sandstones (south eastern France). *Sed. Geol.*, **344**, 382–407.

Tinterri, R., **Mazza, T.** and **Magalhaes, P.M.** (2022) Contained-Reflected Megaturbidites of the Marnoso-arenacea Formation (Contessa Key Bed) and Helminthoid Flysches (Northern Apennines, Italy) and Hecho Group (South-Western Pyrenees). *Front. Earth Sci.*, **10**, 817012.

Van der Merwe, W.C., **Hodgson, D.M.** and **Flint, S.S.** (2009) Widespread syn-sedimentary deformation on a muddy deep-water basin-floor: the Vischkuil Formation (Permian), Karoo Basin, South Africa. *Basin Res.*, **21**, 389–406.

Vinent, O.D., **Andreotti, B.**, **Claudin, P.** and **Winter, C.** (2019) A unified model of ripples and dunes in water and planetary environments. *Nat. Geosci.*, **12**, 345–350.

Wignall, P.B., **Bond, D.P.G.**, **Grasby, S.E.**, **Pruss, S.B.** and **Peakall, J.** (2020) Controls on the formation of microbially-induced sedimentary structures and biotic recovery in the Lower Triassic of Arctic Canada. *Geol. Soc. Am. Bull.*, **132**, 918–930.

Winterer, E.L. (1964) Late Precambrian pebbly mudstone in Normandy, France: Tillite or Tilloid? In: *Problems in Palaeoclimatology* (Ed Nairn, A.E.M.), pp. 159–178. Interscience Publishers, Geneva.

Wizevich, M.C., **Simpson, E.L.**, **Hilbert-Wolf, H.L.** and **Tindall, S.E.** (2016) Development of large-scale seismites in Upper Cretaceous fluvial sandstones in a fault-proximal setting. *Sedimentology*, **63**, 1719–1738.

Yanniotis, S., **Skaltsi, S.** and **Karaburnioti, S.** (2006) Effect of moisture content on the viscosity of honey at different temperatures. *J. Food Eng.*, **72**, 372–377.

Yin, D., **Peakall, J.**, **Parsons, D.**, **Chen, Z.**, **Macdonald Averill, H.**, **Wignall, P.** and **Best, J.** (2016) Bedform genesis in bedrock substrates: insights into formative processes from a new experimental approach and the importance of suspension-dominated abrasion. *Geomorphology*, **255**, 26–38.

Manuscript received 6 November 2023; revision accepted 19 June 2024